sustainability

MDPI

Article

Efficient Operation of the Hybrid Power System Using an Optimal Fueling Strategy and Control of the Fuel Cell Power Based on the Required Power Tracking Algorithm

Nicu Bizon [1,2,3,*], Phatiphat Thounthong [4,5] and Damien Guilbert [5]

1 Faculty of Electronics, Communication and Computers, University of Pitesti, 110040 Pitesti, Romania
2 ICSI Energy, National Research and Development Institute for Cryogenic and Isotopic Technologies, 240050 Ramnicu Valcea, Romania
3 Doctoral School, Polytehnic University of Bucharest, 313 Splaiul Independentei, 060042 Bucharest, Romania
4 Renewable Energy Research Centre (RERC), Department of Teacher Training in Electrical Engineering, Faculty of Technical Education, King Mongkut's University of Technology North Bangkok, 1518, Pracharat 1 Road, Bangsue, Bangkok 10800, Thailand; phatiphat.t@fte.kmutnb.ac.th
5 Groupe de Recherche en Energie Electrique de Nancy (GREEN), Université de Lorraine, GREEN, F-54000 Nancy, France; damien.guilbert@univ-lorraine.fr
* Correspondence: nicu.bizon@upit.ro

Received: 10 October 2020; Accepted: 18 November 2020; Published: 20 November 2020

Abstract: In this paper, four fuel economy strategies using power tracking control of the fuel cell boost converter and fuel cell optimization through the control of the fueling regulators were analyzed. The performance and safe operation in conditions of load disturbances and variations of renewable energy were considered. A benchmark strategy was used as a well-known strategy, which was based on the static feed-forward control of the fueling regulators. One of the four strategies is new and was based on switching the optimization reference to air and fuel regulators based on a threshold of the required power from the fuel cell system. The advantages of using the power tracking control and the optimization based on two variables instead of one are highlighted in sizing the battery capacity and its lifetime, and obtaining fuel economy respectively. The percentages of fuel economy for the analyzed strategies compared to the reference strategy are between 2.83% and 4.36%, and between 7.69% and 12.94%, in the case of a dynamic load cycle with an average of 5 kW and 2.5 kW, respectively.

Keywords: hybrid power system; nano-grid; fuel cell; fuel economy; power tracking; optimization

1. Introduction

A hybrid power system (HPS) includes renewable energy sources, power generators, DC and AC loads, and energy and power storage devices that ensure the balance of power flows in conditions of stability and safe operation of the entire system [1]. One or more HPSs are usually integrated into a nano-grid or a mini-grid [2]. Depending on the size (kW), capability, and complexity of a grid, they are classified into mini-grids, micro-grids, nano-grids, and pico-grids [3]. For example, a nano-grid can produce or consume energy in interaction with other mini-, micro- or nano-grids [4]. Thus, the HPS based on fuel cell (FC) systems as backup energy source proposed in this study can emulate the operation of a nano-grid by including the power demand on the AC bus (from AC load and power exchanged with the grid in grid-connected mode) in the power profile of the DC load.

Due to the growing global energy demand in recent years [5], the reduction of fossil fuel resources [6] and the increase in greenhouse gas emissions have been contributing to climate change

and global warming [7]. Hence, sustainable energy development policies have been imposed [8]. The increasing use of renewable energy sources (RES) in the last decade has clearly shown that they are a sustainable option for providing the energy needed for decades to come [9].

However, it is worth mentioning that each RES has a variable profile (even intermittent), so regardless of how the combination of RESs available in a certain location (where in addition to solar energy, there can be energy generated by wind, rivers, tides, biomass and so on) the balance of power flows must be compensated to ensure the stability of HPS [10]. Given that FC technology has matured and costs have been declining year by year, the FC system is frequently used as an auxiliary power source (instead of a diesel generator) to reduce the battery capacity. However, since fuel cells feature slow dynamics, they cannot be employed to respond to dynamic solicitations from the loads connected to the DC bus. Therefore, the use of a hybrid energy storage system (ESS) such as the combination batteries/ultracapacitors is required to compensate the dynamic operations [11].

If FC HPS is not connected to the grid (being included in a nano-grid), it is recommended that the excess renewable energy be stored in hydrogen tanks using an electrolyzer [12]. If FC HPS is connected to the grid, this surplus energy can be sold on the energy market when the price is the best.

This results in a hybridization of the grids by including complementary technologies for energy generation and storage [13], with the aim of attenuating the variability of RES power by integrating complementary technologies and efficient control of power converters [14]. Thus, the objectives of this paper are as follows:

1. To analyze four fuel economy strategies using power tracking control (PTC) of the FC boost converter and optimization through global extremum seeking (GES)-based control of the fueling regulators, as (1) performance compared with a benchmark strategy, and (2) safe operation in conditions of load disturbances and variations of renewable energy;
2. To design and test a new fuel economy strategy using PTC and optimization through GES-based control that is switched to the fuel and air by using a tuned power threshold to maximize the fuel economy;
3. To highlight the operation of the HPS in conditions of load disturbances and variations of renewable energy under PTC and related advantages in sizing the battery capacity and its lifetime.

Secondary objectives are focused on:

1. Identifying performance indicators to recognize the strategies of a subclass among other subclasses belonging to the same class of optimization strategies;
2. Proposing indicators that will allow estimation of fuel consumption over a predicted load cycle up to the first refueling station if the consumption during a standard load cycle is known.

The novelty of this study compared to other similar studies (including those published by the authors) is given by the following elements presented and validated in this study:

1. A new fuel economy strategy based on switching the optimization reference to air and fuel regulator considering a threshold of the required power from the fuel cell system is proposed and analyzed as performance compared to the original reference strategies and a commercial benchmark strategy.
2. Considering a variable power profile for the load demand and the renewable power, the advantages in design and operation of the battery stack due to the charge-sustained mode for battery using the new power tracking control proposed for the FC system are highlighted as follows: a reduced capacity and size is needed for the battery; an increased battery lifespan could be obtained avoiding the frequent charge-discharge cycles that appear in other strategies proposed in the literature; maintenance costs can be reduced (due to the fact that it is not necessary to monitor the state of charge (SOC) of the battery, because the final SOC will be almost equal to the initial SOC).

3. The advantages of using a new optimization fuel strategy based on two variables instead of one are highlighted by fuel economy obtained under variable power profile for the load demand and the renewable power.
4. New performance indicators to recognize the strategies of a subclass among other subclasses are proposed and validated using the four strategies analyzed here.

So, besides the introduction, the paper is structured into a further four sections as follows. Section 2 presents the HPS model, detailing in subsections the PTC, GES control, and fueling strategies analyzed in this paper. Section 3 presents the results obtained in stationary and dynamic regimes of HPS. Finally, Section 4 comparatively analyzes the results and Section 5 concludes the paper.

2. Modeling of the Hybrid Power System

The structure of the hybrid power system (HPS) is shown at the top of Figure 1, which presents the HPS diagram and details the following subsystem: the energy management unit that contains the PTC, the optimal fueling strategy, the real-time optimization algorithm, and the semi-active ESS topology. The renewable power level on the DC bus is controlled by the k_{RES} parameter (see the HPS diagram at the top of Figure 1). The FC power will be generated based on the PTC to compensate the power flow balance on the DC bus and operate the battery in charge-sustained mode.

The inverter system and AC load have been equated at the DC bus level with a DC load. DC load is modeled by a controlled current source, resulting in a dynamic power (P_{load}) required from the power sources connected to the DC bus (see for example, Figure 2). Non-polluting energy sources such as photovoltaic panel arrays [15] and wind turbine farms [16] may provide renewable energy, but the available renewable power profile is variable (depending on weather, season, etc.) [17], and the DC bus power balance must be dynamically compensated by the ESS [18]. Consequently, it will result in a variable profile for ESS power due to the changed power with DC bus, with frequent charge-discharge cycles, which reduce the battery life [19]. Furthermore, battery pack capacity must be oversized to provide the DC power needed under a variable power profile from RES, such as that shown in Figure 3a or Figure 4a (P_{RES1} and P_{RES2} for $k_{RES} = 1$ and $k_{RES} = 2$). RES is also modeled by a controlled current source to easily change the RES power profile.

The battery/ultracapacitors hybrid ESS (see bottom of the Figure 1) uses a semi-active topology (with the battery connected directly to the DC bus and the ultracapacitors stack connected to the DC bus via a bidirectional DC-DC power converter), which is the most widely used in the literature because it ensures a trade-off between cost, performance, and flexibility in control.

The ESS power is shown in Figures 3b and 4b for $k_{RES} = 1$ and $k_{RES} = 2$, respectively. In the first case, the battery is discharged and the state-of-charge (SOC) will decrease. In the second case, the battery operates in charge-discharge cycles, but in average value (AV) it seems to operate in charge-sustained mode (so, the final SOC will be approximately equal with the initial SOC of 80%). However, it is observed that there are charge and discharge cycles that must be taken into account in the design of the battery capacity. Note that $P_{load(AV)} = 5$ kW, $P_{RES1(AV)} \cong 2.5$ kW, and $P_{RES2(AV)} \cong 5$ kW, so $P_{ESS1(AV)} \cong 2.5$ kW, and $P_{ESS2(AV)} \cong 0$.

Battery pack operation in charge-sustained mode with SOC variations within the admissible limits due to a reduced level of the ESS power exchanged with DC bus has the following advantages: no battery capacity oversizing and SOC monitoring is required.

Therefore, it is necessary to use a backup energy source to operate the battery pack in charge-sustained mode ($P_{ESS(AV)} \cong 0$) with a reduced level of the ESS power exchanged with DC bus [20]. If a clean solution is desired, then the fuel cell (FC) system can be used [21].

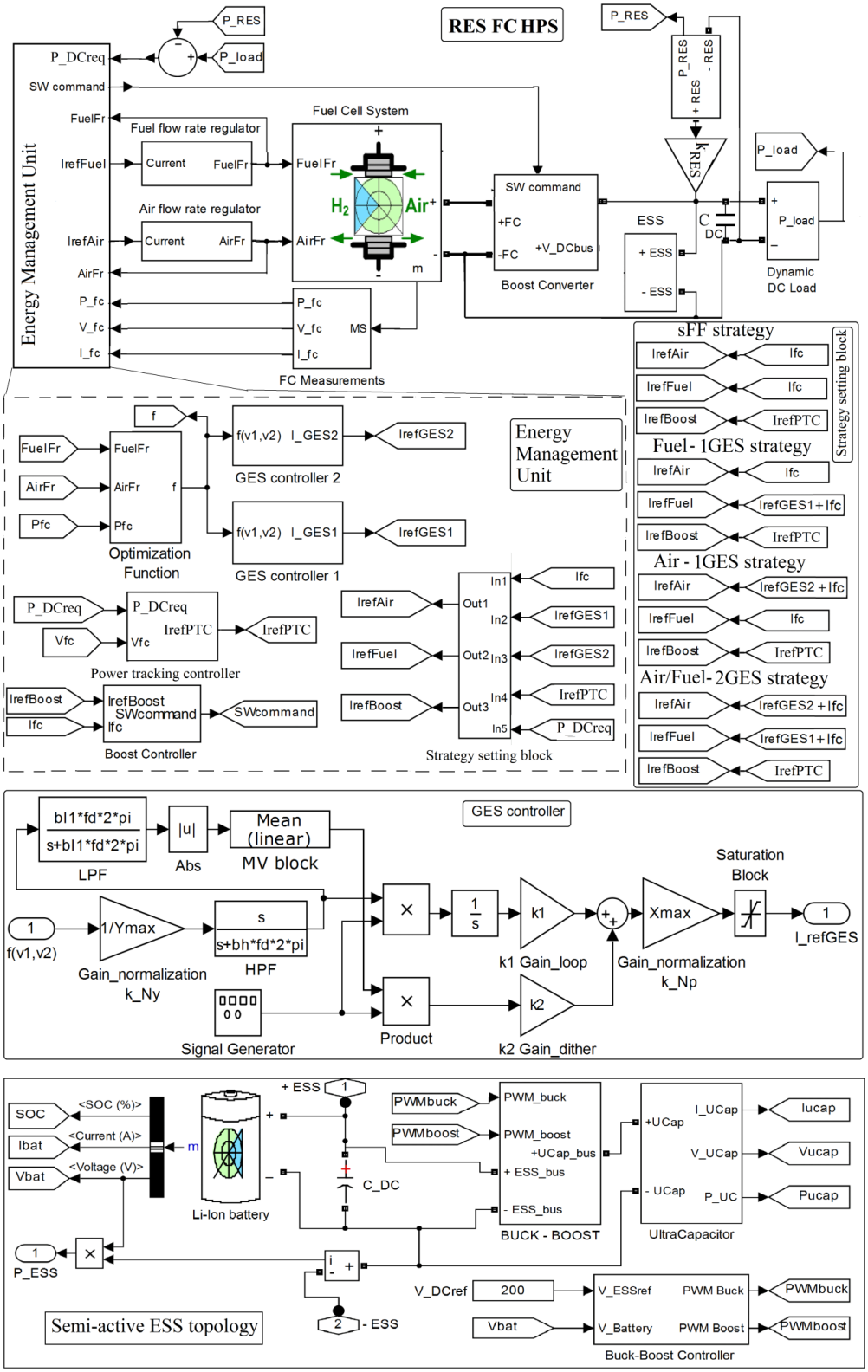

Figure 1. Hybrid power system (HPS).

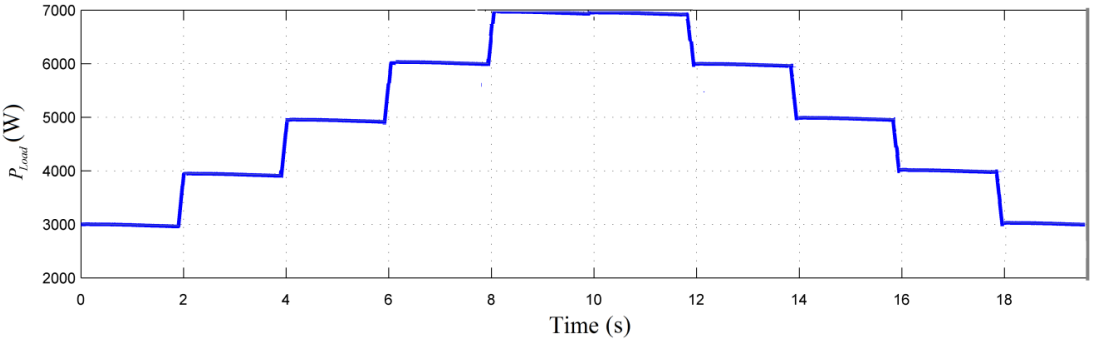

Figure 2. Load power profile.

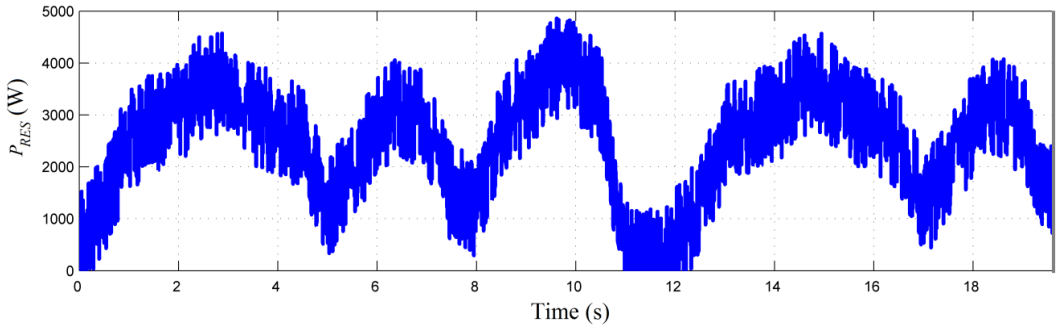

(**a**)

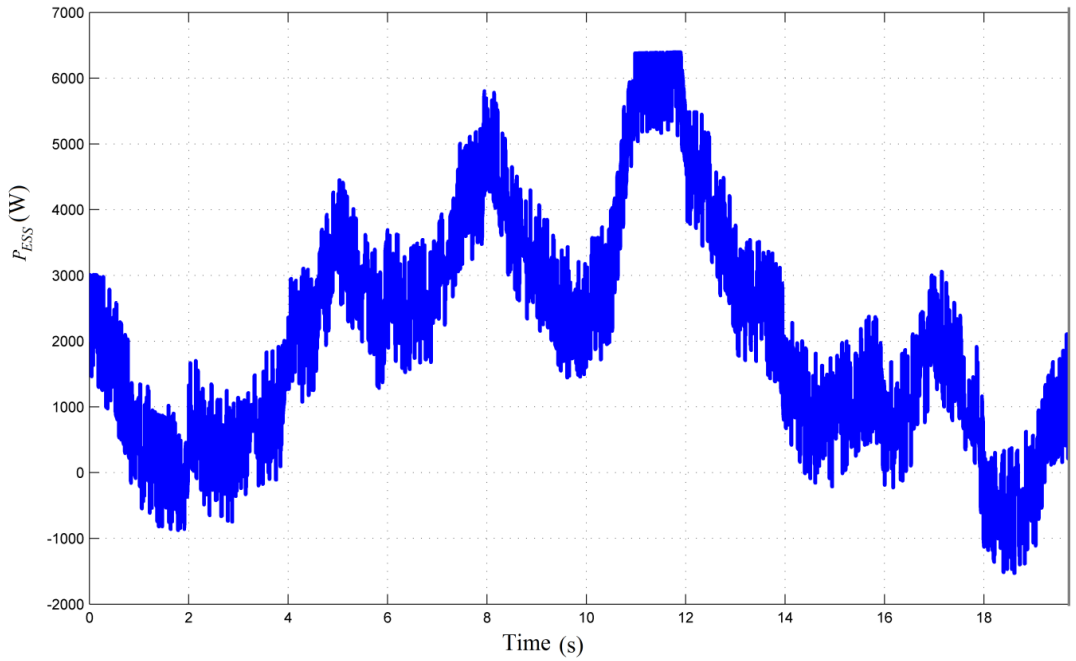

Figure 3. The first power profile for the renewable energy source (RES), P_{RES1} for $k_{RES} = 1$ (**a**) and energy storage system (ESS), P_{ESS1} for $k_{RES} = 1$ (**b**).

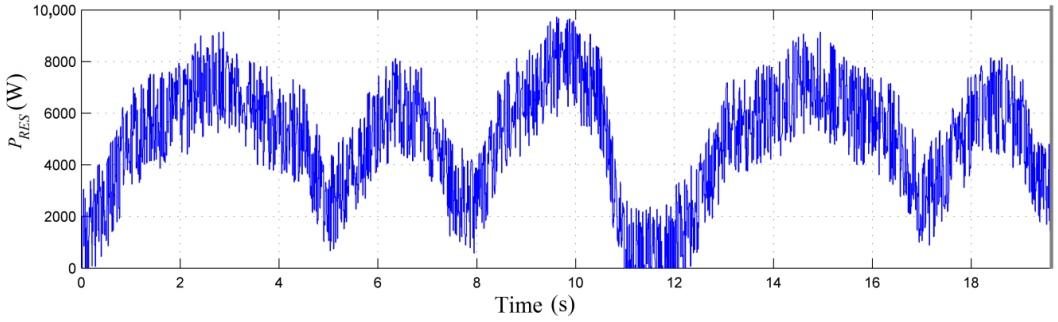

(**a**)

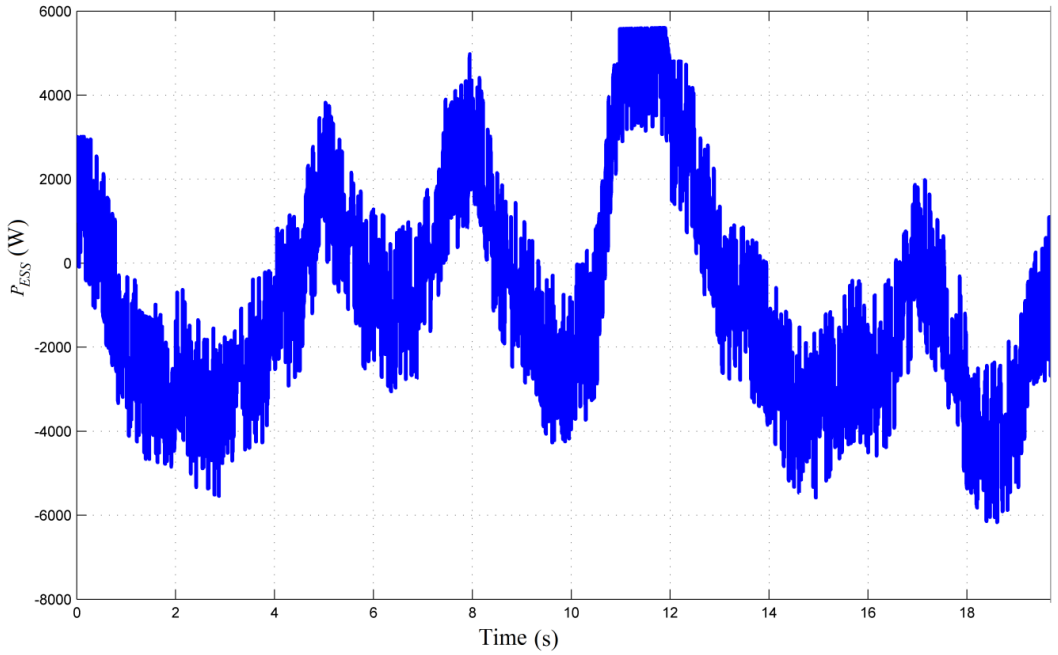

(**b**)

Figure 4. The second power profile for the RES, P_{RES2} for $k_{RES} = 2$ (**a**) and ESS, P_{ESS2} for $k_{RES} = 2$ (**b**).

In this study, a proton-exchange membrane fuel cell (PEMFC) and an electrolyzer was used. The electrolyzer must be supplied with excess power ($P_{RES} - P_{load}$) > 0, when the FC system does not have to generate power (being switched off or operating in standby mode) [22]. If $P_{RES} < P_{load}$ and $P_{ESS(AV)} \cong 0$, then the FC system must generate the power requested to compensate for the DC power flow balance ($P_{DCreq} = P_{load} - P_{RES} > 0$). Power P_{DCreq} is generated via a DC-DC boost converter (with efficiency η_{Boost}). Thus, FC net power must be $P_{FCnet} = P_{DCreq}/\eta_{Boost}$ under the PTC that generates the switching (SW) command.

The oxygen and hydrogen flow rates (*AirFr* and *FuelFr*) of the PEMFC system is controlled with air and fuel regulators having as references $I_{ref(Air)}$ and $I_{ref(Fuel)}$ [23]:

$$AirFr = \frac{60000 \cdot R \cdot (273 + \theta) \cdot N_C \cdot I_{ref(Air)}}{4F \cdot (101325 \cdot P_{f(O2)}) \cdot (U_{f(O2)}/100) \cdot (y_{O2}/100)} \quad (1)$$

$$FuelFr = \frac{60000 \cdot R \cdot (273 + \theta) \cdot N_C \cdot I_{ref(Fuel)}}{2F \cdot (101325 \cdot P_{f(H2)}) \cdot (U_{f(H2)}/100) \cdot (x_{H2}/100)} \quad (2)$$

where $N_C, \theta, U_{f(H2)}, U_{f(O2)}, P_{f(H2)}, P_{f(O2)}, x_{H2}, y_{O2}$ are default parameters explained in [24].

For a given FC net power under PTC reference ($I_{ref(PTC)}$), the fuel consumption can be minimized by using an optimal fueling strategy to set in real-time the references $I_{ref(Air)}$ and $I_{ref(Fuel)}$ [25].

The aforementioned references ($I_{ref(PTC)}$, $I_{ref(Air)}$ and $I_{ref(Fuel)}$) are outputs of the energy management unit that contains the PTC, the optimal fueling strategy, and the real-time optimization algorithm. The design of the energy management unit will be detailed in the next sections.

2.1. Control of the Fuel Cell Power Based on the Required Power Tracking Algorithm

The PTC has been designed based on the DC power flow balance as follows:

$$C_{DC}u_{DC}du_{DC}/dt = p_{DC} + p_{RES} + p_{ESS} - p_{Load} \quad (3)$$

where $p_{DC} = \eta_{boost}p_{FCnet}$ is the power generated by the FC system via DC-DC boost converter, p_{FCnet} is FC net power, p_{RES} is RES power, p_{ESS} is ESS power and p_{Load} is load power.

DC voltage u_{DC} is regulated to V_{DCref} = 200 V by controlling the power exchanged by a 50 F ultracapacitors (UC) stack with DC bus via a bidirectional DC-DC converter and filtered by a 0.01 F capacitor (C_{DC}). Therefore, a semi-active ESS topology was designed [20,21] and implemented here using a 100 Ah lithium-ion battery pack and a 50 F UC stack (see bottom of Figure 1).

If

$$p_{DC} = \eta_{Boost}p_{FCnet} = p_{DCreq} = p_{Load} - p_{RES} \quad (4)$$

then

$$C_{DC}u_{DC}du_{DC}/dt = p_{ESS} \quad (5)$$

So, on average value (AV):

$$P_{ESS(AV)} = 0 \quad (6)$$

However, due to implementation of the optimal fueling strategy, the FC net power may differ a bit to the value resulting from (4), being approximate to that value:

$$p_{FCnet} \cong \frac{p_{Load} - p_{RES}}{\eta_{Boost}} \Rightarrow I_{FC} \cong \frac{p_{Load} - p_{RES}}{V_{FC}\eta_{Boost}} \quad (7)$$

So, the FC current reference ($I_{ref(PTC)}$) obtained from the PTC will be given by (8):

$$I_{ref(PTC)} = \frac{p_{Load} - p_{RES}}{V_{FCnet}\eta_{Boost}} = \frac{p_{DCreq}}{V_{FCnet}\eta_{Boost}} \quad (8)$$

The optimal fueling strategy is selected using the strategy-setting block (see the energy management unit presented in the middle of Figure 1). Note that for all strategies, the boost controller has FC current (I_{FC}) as one input and the second input ($I_{ref(Boost)}$) is set to PTC reference ($I_{ref(PTC)}$). Thus, using, for example, a boost controller with 0.1 A hysteresis, the FC current will track the PTC reference.

The battery pack and ultracapacitors stack will compensate for the energy and power imbalances in DC power flow balance (3) due to the implementation of the optimization strategy and slow power response of the FC system (using 100 ms time constant and 100 A/s slope limiters in the fueling regulators).

The references $I_{ref(Air)}$ and $I_{ref(Fuel)}$ were specifically established for each fueling strategy analyzed in this study (see the strategy-setting block presented in the middle of Figure 1), as will be presented in the next section.

2.2. Fueling Strategies

In order to compare the performance of the fueling strategies analyzed in this study, a well-known control strategy, applied in many commercial applications and known in the literature as the static feed-forward (sFF) control [26], will be used as a reference.

In sFF strategy, the fueling regulators are both controlled by FC current, so the references $I_{ref(Air)}$ and $I_{ref(Fuel)}$ are set as follows:

$$I_{ref(Fuel)} = I_{FC}\ ,\ I_{ref(Air)} = I_{FC} \tag{9}$$

Optimizing the operation of the FC system referred in this study to the minimization of total fuel consumption ($Fuel_T = \int FuelFr(t)dt$) using an optimization function given by (10):

$$f(x, AirFr, FuelFr, P_{load}, P_{RES}) = 0.5 \cdot P_{FCnet} + k_{fuel} \cdot Fuel_{eff} \tag{10}$$

where x is the vector of FC state variables [26], $Fuel_{eff} \cong P_{FCnet}/FuelFr$ is the fuel consumption efficiency and k_{fuel} = 25 (Lpm/W) to minimize the fuel consumption. This value of the k_{fuel} parameter has been obtained by sensitivity analysis performed in the range 0–50 (Lpm/W) for the optimization function given by (10) [23,25].

The global extremum seeking (GES) [27] was selected as the search algorithm of the maximum for function f in conditions of load disturbances and variations of renewable energy. The search variables were $v_1 = AirFr$ and $v_2 = FuelFr$ and the GES model (which is shown in the bottom of Figure 1) will be detailed in the next section.

For the fueling strategies analyzed in this study, the references $I_{ref(GES1)}$ and $I_{ref(GES2)}$ generated by GES controllers were specifically established to the references $I_{ref(Air)}$ and $I_{ref(Fuel)}$ as follows.

For the strategy using optimization through GES-based control of the fuel regulator (labelled below as Fuel-1GES strategy), the settings were:

$$I_{ref(Fuel)} = I_{FC} + I_{ref(GES1)},\ I_{ref(Air)} = I_{FC} \tag{11}$$

For the strategy using optimization through GES-based control of the air regulator (labelled below as Air-1GES strategy), the settings were:

$$I_{ref(Air)} = I_{FC} + I_{ref(GES2)},\ I_{ref(Fuel)} = I_{FC} \tag{12}$$

For the strategy using optimization through GES-based control of both air and fuel regulators (labelled below as Air/Fuel-2GES strategy), the settings were:

$$I_{ref(Fuel)} = I_{FC} + I_{ref(GES1)},\ I_{ref(Air)} = I_{FC} + I_{ref(GES2)} \tag{13}$$

A new strategy was proposed using optimization through GES-based control switched to the fuel and air (labelled below as Air/Fuel-2GES SW strategy). A power threshold to maximize the fuel economy was used, so the settings are given by (14):

$$I_{ref(Fuel)} = \begin{cases} I_{FC},\ if\ P_{DCreq} \le P_{ref} \\ I_{FC} + I_{ref(GES1)},\ if\ P_{DCreq} > P_{ref} \end{cases},\ I_{ref(Air)} = \begin{cases} I_{FC} + I_{ref(GES2)},\ if\ P_{DCreq} \le P_{ref} \\ I_{FC},\ if\ P_{DCreq} > P_{ref} \end{cases} \tag{14}$$

Air/Fuel-2GES SW strategy uses the best fuel saving strategy between Fuel-1GES and Air-1GES strategies on power ranges defined by the threshold P_{ref} (see Figure 5). Therefore, an increase in fuel economy is expected (see the results section), but two GES controllers are used instead of one as used in Fuel-1GES strategy or Air-1GES SW strategy.

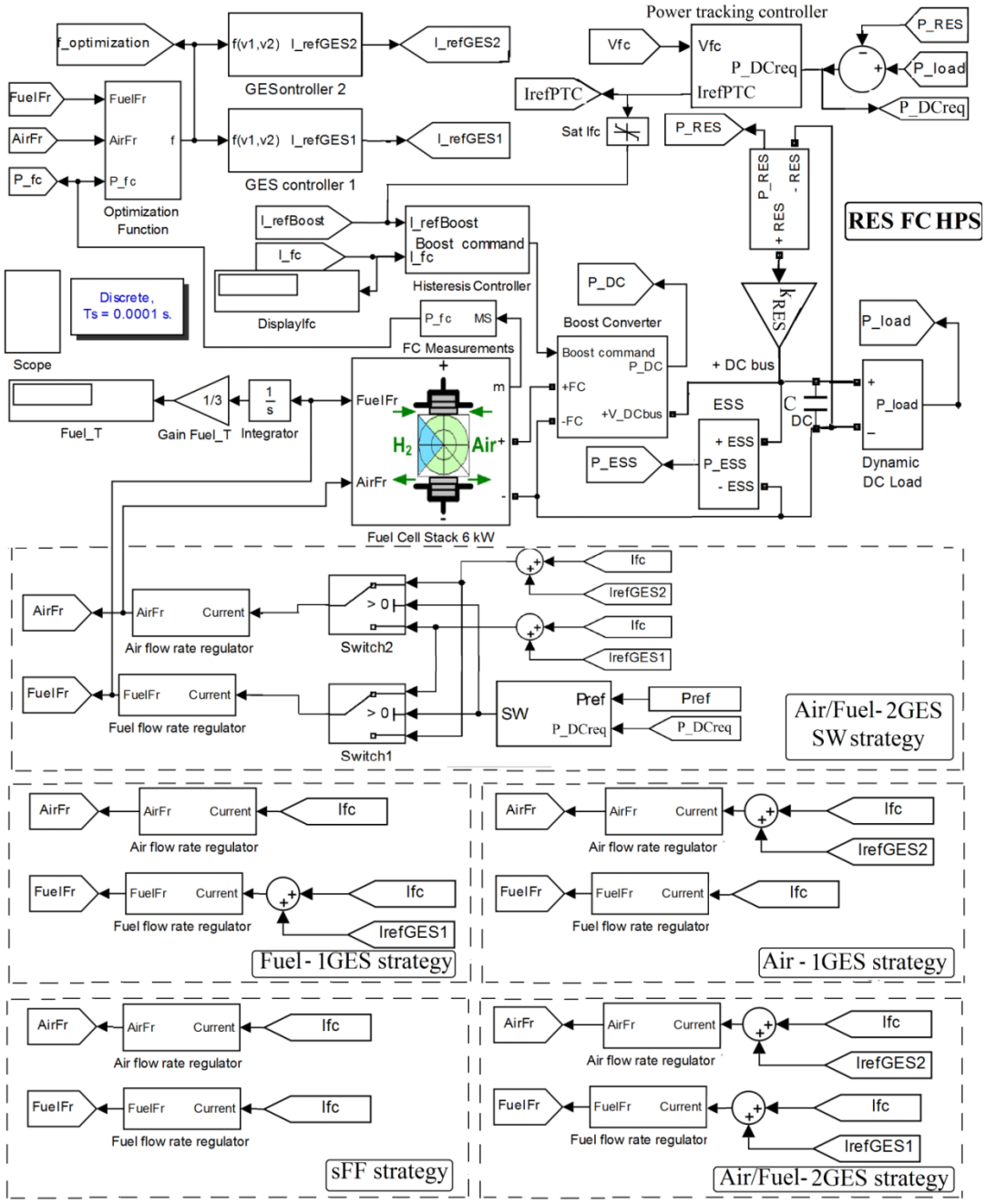

Figure 5. Diagram of the proposed strategies.

The additional use of an optimization controller will increase the complexity of the strategy somewhat, even if the optimization controller based on the GES scheme is not difficult to implement [28,29] (see next section).

2.3. GES-Based Optimization Controller

The GES-based optimization controller is presented at the bottom of Figure 1. Signals are processed based on the operational relationships (15) [30]:

$$y = f(v_1, v_2), y_N = k_{Ny} \cdot y \tag{15a}$$

$$\dot{y}_f = -\omega_h \cdot y_f + \omega_h \cdot y_N,\ y_{HPF} = y_N - y_f,\ \dot{y}_{BPF} = -\omega_l \cdot y_{BPF} + \omega_l \cdot y_{HPF} \tag{15b}$$

$$\omega_h = b_h\omega,\ \omega_l = b_l\omega,\ \ s_d = \sin(\omega t),\ \omega = 2\pi f_d \tag{15c}$$

$$y_{DM} = y_{BPF} \cdot s_d, \dot{y}_{Gradient} = y_{DM}, p_1 = k_1 \cdot y_{Gradient} \tag{15d}$$

$$y_M = \left|\frac{1}{T_d} \cdot \int y_{BPF} dt\right|,\ p_2 = k_2 \cdot y_M \cdot s_d \tag{15e}$$

$$I_{ref(GES)} = k_{Np} \cdot (p_1 + p_2) \tag{15f}$$

The step in signals processing and used parameter are follows [30]:

- Normalization of FC power (y = p_{FCnet}) is performed using k_{Ny} = 1/1000;
- Approximation the first harmonic (y_{BPF}) is performed with a band-pass filter having the cut-off frequencies $\omega_l = b_l\omega$ and $\omega_h = b_h\omega$, where $\beta_l = 1.5$ and $\beta_h = 0.1$.
- Two sinusoidal dithers, $s_{d1} = \sin(\omega_1 t)$ and $s_{d2} = \sin(\omega_2 t)$ are used (with f_{d1} = 50 Hz and f_{d2} = 100 Hz, where $f_d = \omega/2\pi$) to perform demodulation (y_{DM});
- Signal y_{DM} is integrated to obtain the search gradient ($y_{Gradient}$);
- The tracking signal (p_1) and the location signal (p_2) are tuned using k_1 = 1 and k_2 = 2;
- Normalization of the search signal ($p = p_1 + p_2$) is performed using k_{Np} = 20.

The values of the normalization gains k_{Ny} and k_{Np} were chosen in correlation with the range of the FC power, respectively the search range for the references $I_{ref(GES1)}$ and $I_{ref(GES2)}$ generated by GES controllers [30], which established the references $I_{ref(Air)}$ and $I_{ref(Fuel)}$ as mentioned above. It is worth mentioning the 99.9% tracking accuracy and very low power ripple obtained in stationary regimes [31]. The efficient and safe operation of the FC system using the strategies mentioned above were evaluated in stationary and dynamic regimes, considering the fuel economy and the oxygen excess ratio as an indicator of performance and health respectively [32].

The initial simulation conditions are as follows: the initial battery SOC of 80%, the initial voltage on the ultracapacitors stack and DC capacitor of 100 V (V_{UC} (0) = 100 V) and 200 V (V_{C_DC} (0) = 200 V), and initial FC current of 0 A (I_{FC} (0) = 0 A) in order to highlight the initial transitory regime. Different values were considered for the initial values mentioned above. A value of the FC current close to the FC current reference ($I_{ref(PTC)}$) given by (8) reduced the initial transitory regime.

2.4. Oxygen Excess Ratio

The oxygen excess ratio (*OER*) was evaluated using (16) [33]:

$$OER = \frac{c_3 \cdot I_{FC}^3 + c_2 \cdot I_{FC}^2 + c_1 \cdot I_{FC} + c_0}{d_1 \cdot I_{FC} + d_0} \tag{16}$$

where: $c_0 = 402.6$, $c_1 = 8.476 \cdot 10^{-5}$ $[1/A]$, $c_2 = -0.81252$ $[1/A^2]$, $d_3 = 0.02673$ $[1/A^3]$, $d_0 = 0.997$, and $d_1 = 61.38$.

The obtained results in stationary and dynamic regimes will be presented in the next sections.

3. Results

3.1. Performance of Strategies Fuel-1GES, Air-1GES and Air/Fuel-2GES SW

The performance of strategies Fuel-1GES, Air-1GES, and Air/Fuel-2GES SW were analyzed for different levels of load by total fuel consumption during 20 s (see Table 1). The P_{ref} threshold for best fuel economy should be chosen around 3 kW (see Figure 6). The values in the last column are summarized for P_{ref} = 3.2 kW.

Table 1. Fuel consumption of strategies Fuel-1GES, Air-1GES, and Air/Fuel-2GES.

P_{load}	$\Delta Fuel_{T(Air\text{-}1GES)}$	$\Delta Fuel_{T(Fuel\text{-}1GES)}$	$\Delta Fuel_{T(Air/Fuel\text{-}2GES)}$
(kW)	(L)	(L)	(L)
2	1.22	−0.09	−0.09
3	−0.25	−0.24	−0.24
4	−0.71	−0.25	−0.71
5	−1.03	−0.46	−1.03
6	−2.08	−1.58	−2.08
7	−10.56	−4.24	−10.56
8	−22.92	−18.48	−22.92

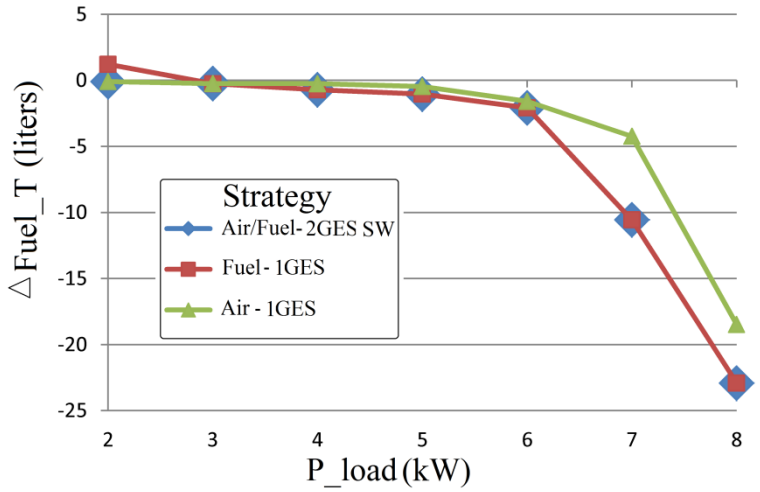

Figure 6. Fuel consumption of strategies Fuel-1GES (global extremum seeking), Air-1GES and Air/Fuel-2GES.

Thus, an increase in fuel economy is expected during dynamic load cycles with levels in the range of zero power to maximum power.

The performance of the strategies mentioned above were evaluated using the load cycle shown in Figure 2. The expected increase in fuel economy will be highlighted in the next section.

3.2. Fuel Consumption for FC HPS (with k_{RES} = 0)

Fuel consumption during the load cycle of 20 s shown in Figure 2 is reported in the first row of Table 2 for strategies sFF, Fuel-1GES, Air-1GES, Air/Fuel-2GES SW, and Air/Fuel-2GES. The fuel economy compared to sFF strategy is presented in the second row of Table 2 using (17).

$$\Delta Fuel_{T(strategy)} = Fuel_{T(sFF)} - Fuel_{T(strategy)} \quad (17)$$

Table 2. Fuel consumption, fuel economy, and percentages of fuel economy compared to $Fuel_{T(sFF)}$ (k_{RES} = 0) during the load cycle shown in Figure 2.

Strategy / Parameter (Unit)	sFF	Fuel-1GES	Air-1GES	Air/Fuel-2GES SW	Air/Fuel-2GES
$Fuel_{T(strategy)}$ (liters)	286.5	278.4	279.4	275.2	274
$\Delta Fuel_{T(strategy)}$ (liters)	0	8.1	7.1	11.3	12.5
$\%Fuel_{T(strategy)}$ (%)	0	2.83	2.48	3.94	4.36

The last row of Table 2 presents the percentages of fuel economy compared to $Fuel_{T(sFF)}$, evaluated by using (18):

$$\%Fuel_{T(strategy)} = 100 \cdot \left(\frac{Fuel_{T(sFF)} - Fuel_{T(strategy)}}{Fuel_{T(sFF)}} \right) \quad (18)$$

As was expected, the fuel economy increased for all strategies compared to sFF strategy and for Air/Fuel-2GES SW strategy compared to the strategies Fuel-1GES and Air-1GES.

To highlight other aspects of the analyzed strategies (such as battery operation in charge-sustained mode or values of other performance indicators) and then discuss them comparatively in the discussion section, the behavior of the FC RES HPS using $k_{RES} = 0$ and strategies sFF, Fuel-1GES, Air-1GES, and Air/Fuel-2GES is presented in Figures 7–10 respectively. The graphs show the load power profile (P_{load}), oxygen excess ratio (OER), ESS power (P_{ESS}), airflow rate ($AirFr$), fuel flow rate ($FuelFr$), total fuel consumption ($Fuel_T$), fuel efficiency ($Fuel_{eff}$), and electrical energy efficiency of FC system ($\eta_{sys} \cong P_{FCnet}/P_{FC}$).

The behavior of Air/Fuel-2GES SW strategy is not presented because its operation is based on the switching of strategies Fuel-1GES and Air-1GES depending on the chosen threshold P_{ref}, so the waveforms would evolve in the same logic.

OER varied within the admissible limits for all the analyzed strategies, highlighting a safe operation for the FC system. OER variation will be detailed in Section 3.4 for FC RES HPS with $k_{RES} = 0$ and $k_{RES} = 1$.

ESS power was almost zero during constant load levels (stationary regimes), except for transient regimes when the power balance was dynamically compensated by ESS, highlighting a battery operation in the charge-sustained mode for all the analyzed strategies.

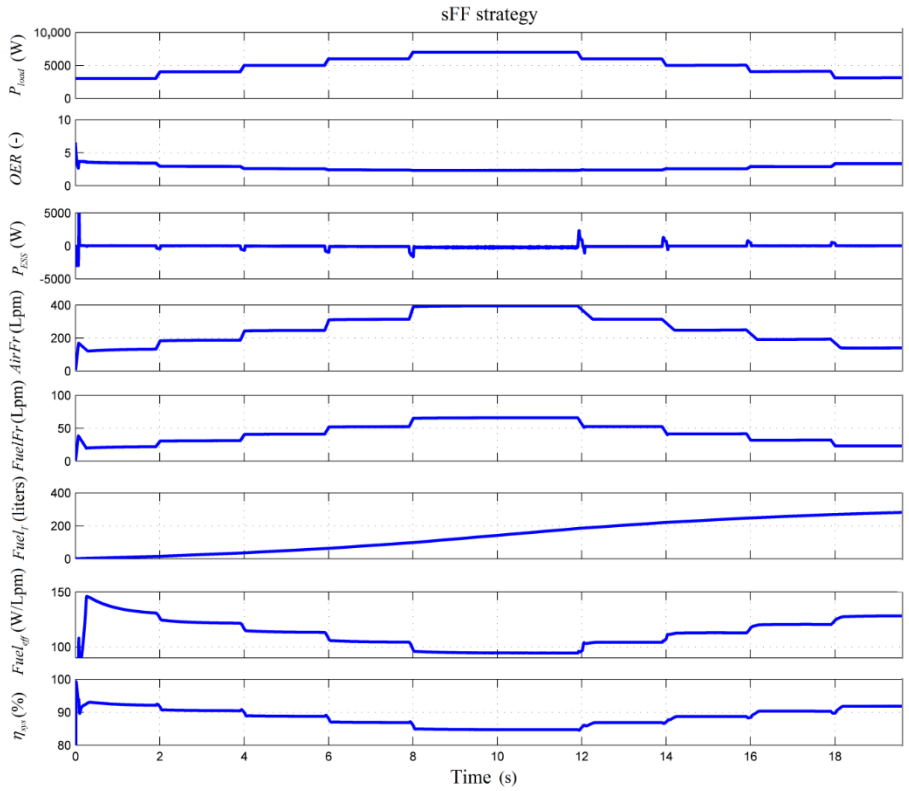

Figure 7. Main waveforms for fuel cell (FC) RES HPS using $k_{RES} = 0$ and static feed-forward (sFF) strategy.

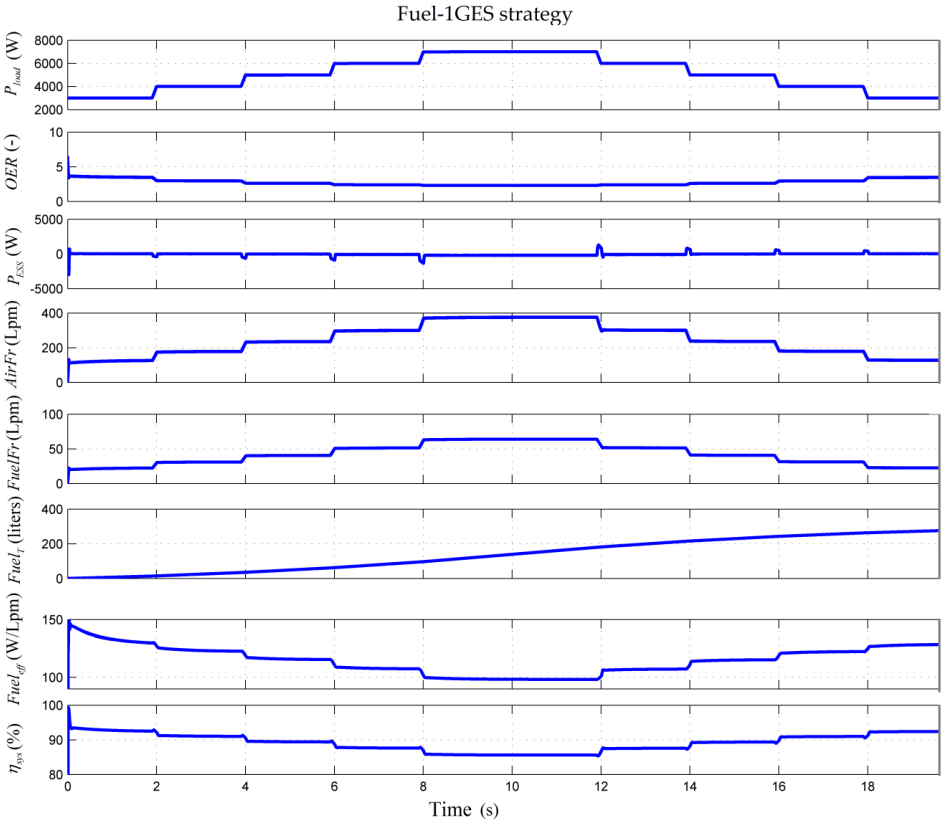

Figure 8. Main waveforms for FC RES HPS using $k_{RES} = 0$ and Fuel-1GES strategy.

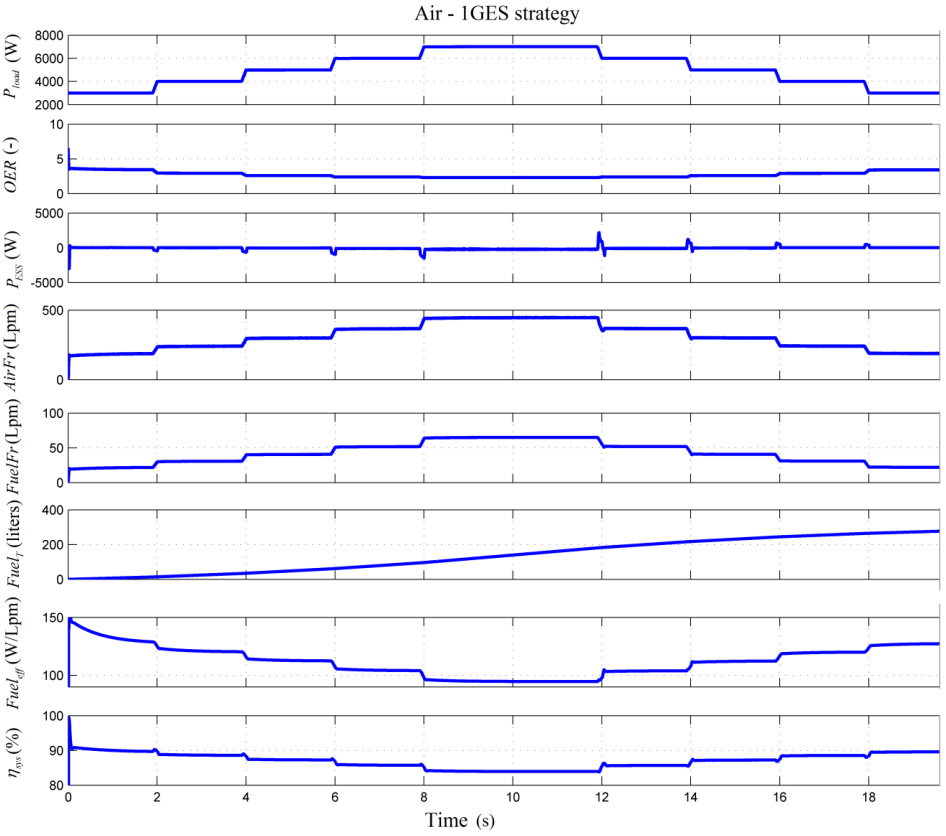

Figure 9. Main waveforms for FC RES HPS using $k_{RES} = 0$ and Air-1GES strategy.

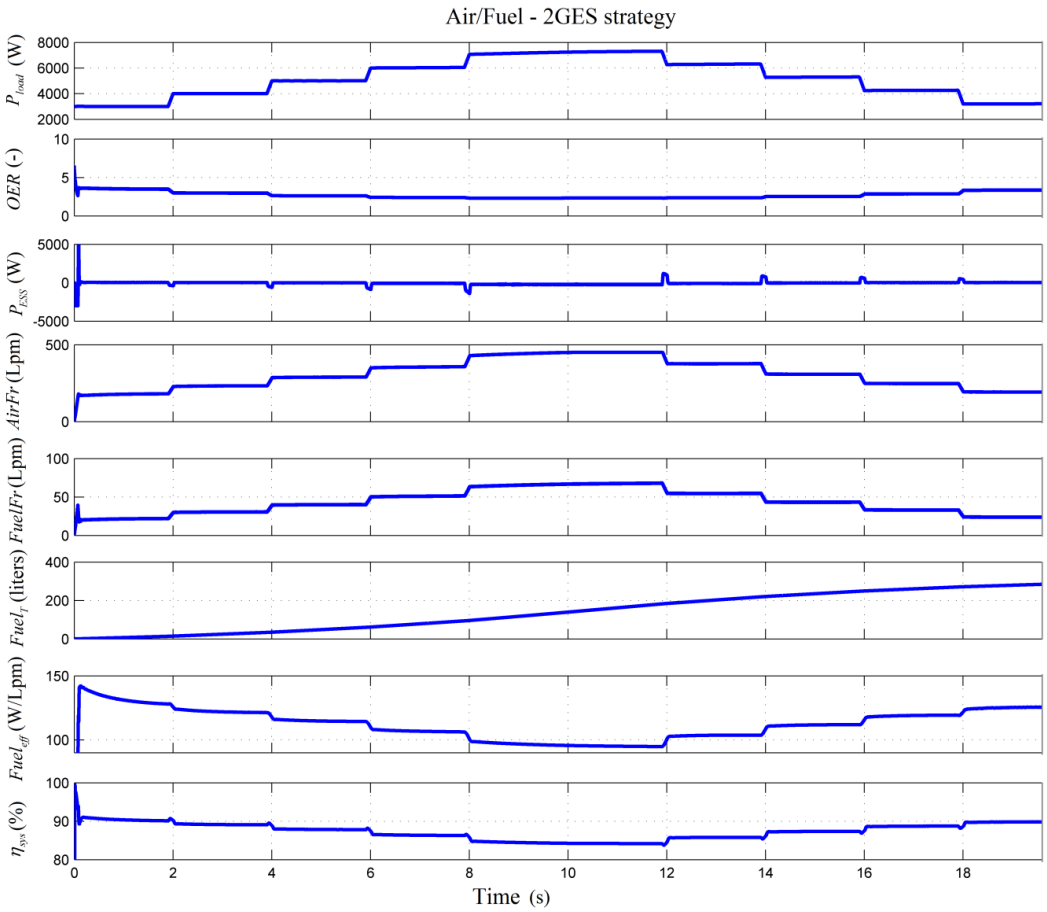

Figure 10. Main waveforms for FC RES HPS using k_{RES} = 0 and Air/Fuel-2GES strategy.

Fueling flow rates (*AirFr* and *FuelFr*) were set by FC current in sFF strategy, so both followed the PTC reference ($I_{ref(PTC)}$). *AirFr* and *FuelFr* were set by FC current in the strategies Fuel-1GES and Air-1GES respectively. So, compared to sFF strategy, minor changes were seen in *FuelFr* and *AirFr* which were used in optimization by the strategies Fuel-1GES and Air-1GES respectively. Air/Fuel-2GES strategy used both fueling flow rates in optimization, so minor changes were seen in both fueling flow rates compared to sFF strategy.

The values of total fuel consumption have been provided in the first row of Tables 2 and 3 for each analyzed strategy and the load cycle of 20 s shown in Figure 2.

Table 3. Fuel consumption, fuel economy, and percentages of fuel economy compared to $Fuel^{RES}_{T(sFF)}$ (k_{RES} = 1) during the load cycle and RES power profile shown in Figures 2 and 3a.

Parameter (Unit) \ Strategy	sFF	Fuel-1GES	Air-1GES	Air/Fuel-2GES SW	Air/Fuel-2GES
$Fuel^{RES}_{T(strategy)}$ (liters)	123.6	113.9	114.1	107.6	108.2
$\Delta Fuel^{RES}_{T(strategy)}$ (liters)	0	9.7	9.5	16	15.4
$\%Fuel^{RES}_{T(strategy)}$ (%)	0	7.85	7.69	12.94	12.46

Two important indicators for evaluating the performance of a strategy are fuel efficiency ($Fuel_{eff}$) and electrical energy efficiency of the FC system ($\eta_{sys} \cong P_{FCnet}/P_{FC}$). An exhaustive analysis (for k_{fuel} = 0, 25, and 50 (Lpm/W) of these performance indicators for seven strategies proposed in the literature

(including strategies Fuel-1GES, Air-1GES, and Air/Fuel-2GES) is presented in [34] compared to the sFF strategy. Here η_{sys} variation is presented to highlight the similar values obtained for FC net power.

FC power variation will be detailed in Section 3.4 for FC RES HPS with $k_{RES} = 0$ and $k_{RES} = 1$. The next section will present the results for FC RES HPS with power support in maintaining to DC power balance from RES, i.e., for $k_{RES} = 1$.

3.3. Fuel Consumption for FC RES HPS with $k_{RES} = 1$

Fuel consumption, the fuel economy, and the percentages of fuel economy compared to the sFF strategy during the 20 s load cycle and RES power profile shown in Figures 2 and 3a are given in Table 3 for strategies sFF, Fuel-1GES, Air-1GES, Air/Fuel-2GES SW, and Air/Fuel-2GES. The fuel economy and the percentages of fuel economy were evaluated using (19) and (20).

$$\Delta Fuel^{RES}_{T(strategy)} = Fuel^{RES}_{T(sFF)} - Fuel^{RES}_{T(strategy)} \tag{19}$$

$$\%Fuel^{RES}_{T(strategy)} = 100 \cdot \left(\frac{Fuel^{RES}_{T(sFF)} - Fuel^{RES}_{T(strategy)}}{Fuel^{RES}_{T(sFF)}} \right) \tag{20}$$

As was expected, fuel consumption decreased due to the contribution of the RES power on DC bus (see the first row of Tables 2 and 3). Note also that the fuel economy increased for the Air/Fuel-2GES SW strategy compared to the strategies Fuel-1GES and Air-1GES (see the second row of Tables 2 and 3). It is also worth mentioning that here the fuel economy was better for the Air-1GES strategy compared to the Fuel-1GES strategy (because the FC power requested was lower due to the contribution of the RES power on DC bus). This also explains better fuel economy for the Air/Fuel-2GES SW strategy compared to the Air/Fuel-2GES strategy (see the second row of Tables 2 and 3).

To compare HPS operation with and without RES power support to DC power balance, the same strategies were used. So, the behavior of the FC RES HPS using $k_{RES} = 1$ and strategies sFF, Fuel-1GES, Air-1GES, and Air/Fuel-2GES is presented in Figures 11–14 respectively. The structure of the graphs is identical to the one mentioned above for Figures 7–10, except for the inclusion of RES power as in the second graph in Figures 11–14.

The values of total fuel consumption presented in the seventh graph have been registered in see the first row of Table 3 for each analyzed strategy.

The following observations can be made for the FC RES HPS using $k_{RES} = 1$:

- ESS power was also almost zero for all strategies, except that it was noisy due to the noise added on RES power, highlighting the battery operation in the charge-sustained mode for FC RES HPS with $k_{RES} = 1$ as well.
- Fueling flow rates (*AirFr* and *FuelFr*) would have evolution as was explained for FC RES HPS with $k_{RES} = 0$, except that for FC RES HPS with $k_{RES} = 1$ the PTC reference and FC currentfollowed the shape of power requested on DC bus, $p_{DCreq} = p_{Load} - p_{RES}$
- It is worth mentioning the low values of the performance indicators ($Fuel_{eff}$ and $\eta_{sys} \cong P_{FCnet}/P_{FC}$) during the operation of the FC system at low power. This mode of operation should be avoided by shutting down the FC system, but shutting down and starting of the FC system are complex processes [35]. An appropriate strategy must therefore be implemented in case the FC system operates for a long time at low power. However, these aspects are not in the objectives of this paper.
- OER varied within the admissible limits for all the analyzed strategies, highlighting a safe operation for FC RES HPS using $k_{RES} = 1$.

So, as it was mentioned, OER variation will be presented and commented on in the next section for FC RES HPS with $k_{RES} = 0$ and $k_{RES} = 1$.

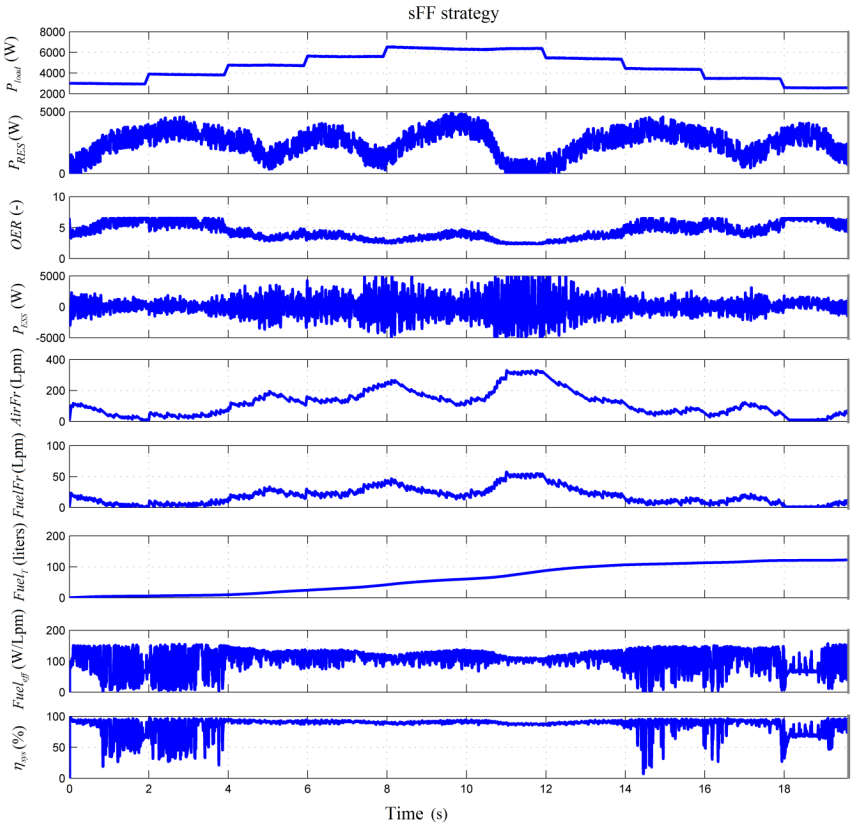

Figure 11. Main waveforms for FC RES HPS using k_{RES} = 1 and sFF strategy.

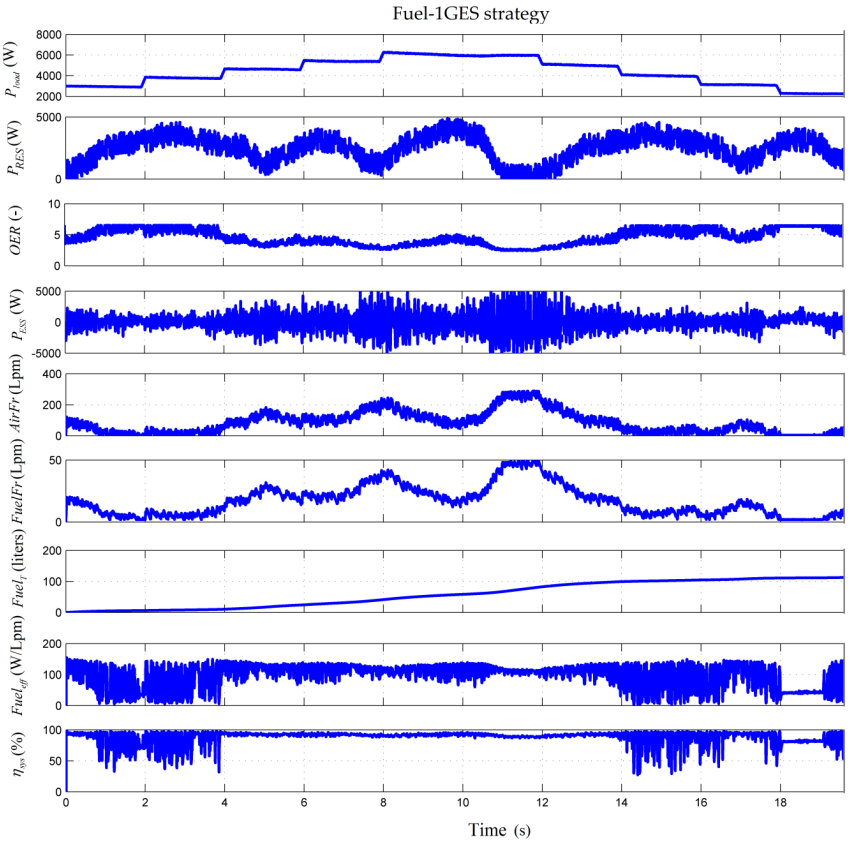

Figure 12. Main waveforms for FC RES HPS using k_{RES} = 1 and Fuel-1GES strategy.

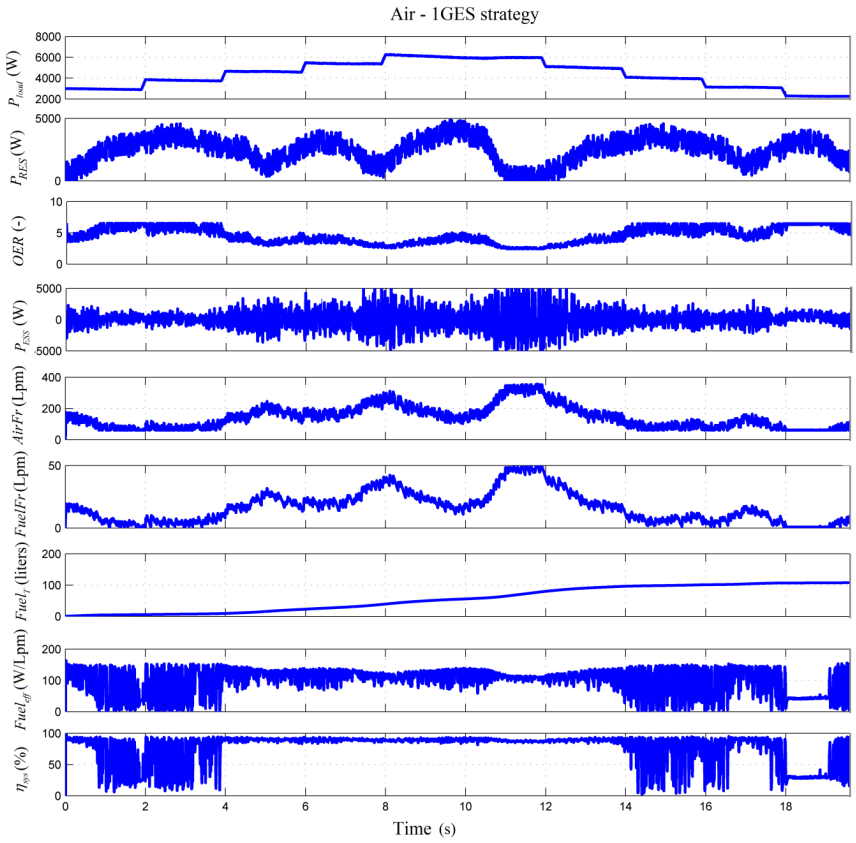

Figure 13. Main waveforms for FC RES HPS using $k_{RES} = 1$ and Air-1GES strategy.

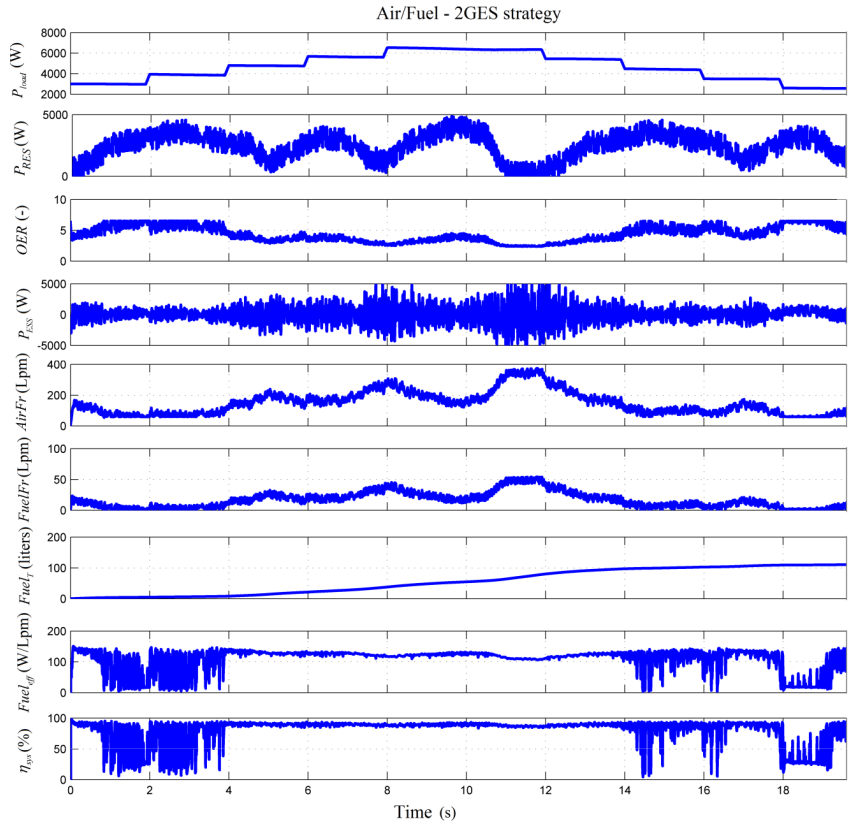

Figure 14. Main waveforms for FC RES HPS using $k_{RES} = 1$ and Air/Fuel-2GES strategy.

3.4. Oxygen Excess Ratio for FC RES HPS with $k_{RES} = 0$ and $k_{RES} = 1$

The oxygen excess ratio of FC RES HPS with $k_{RES} = 0$ is presented in Figure 15 for all strategies. OER varied within the limits of 2.2 and 3.6, which demonstrates the safe operation of HPS without RESs ($k_{RES} = 0$).

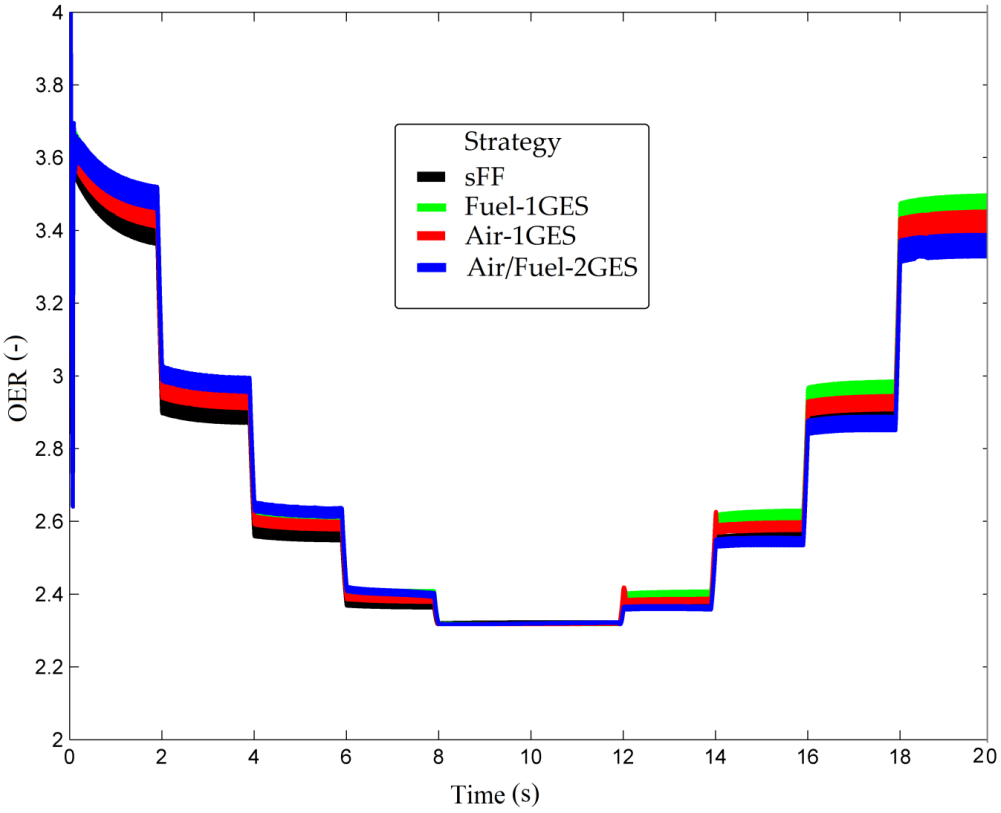

Figure 15. Oxygen excess ratio for FC RES HPS with $k_{RES} = 0$.

Oxygen excess ratio of FC RES HPS with RESs ($k_{RES} = 1$) is presented in Figures 16–19 using the strategies sFF, Fuel-1GES, Air-1GES, and Air/Fuel-2GES respectively. OER variations were represented in different Figures to highlight small variations from one strategy to another (as is the case with ESS power for example). OER varied approximately in the range from 2.3 to 7, so within the allowed limits of safe operation of the FC system.

The same situation (with some minor differences between the representations obtained using the strategies analyzed in this study) applied in the case of FC net power (see next section).

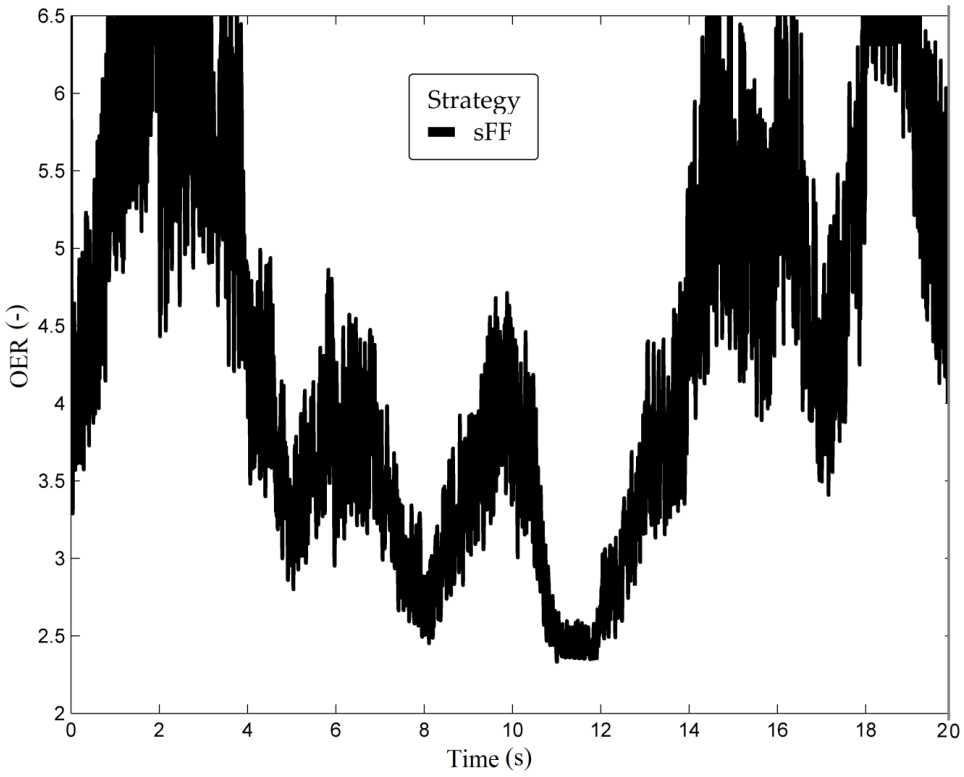

Figure 16. Oxygen excess ratio for FC RES HPS with k_{RES} = 1 and sFF strategy.

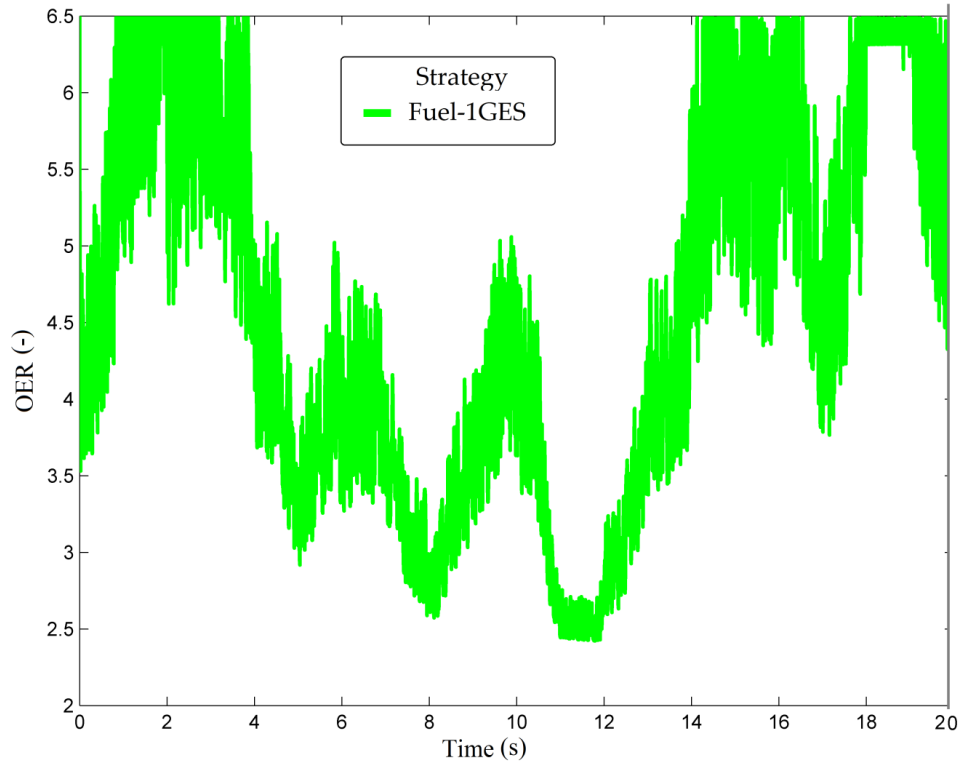

Figure 17. Oxygen excess ratio for FC RES HPS with k_{RES} = 1 and Fuel-1GES strategy.

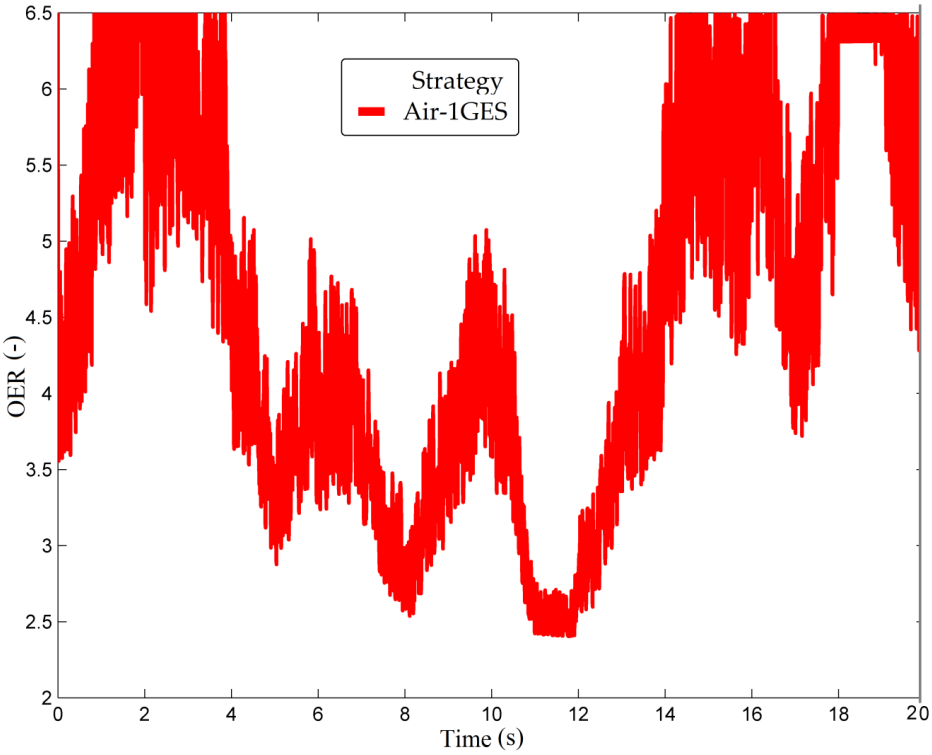

Figure 18. Oxygen excess ratio for FC RES HPS with k_{RES} = 1 and Air-1GES strategy.

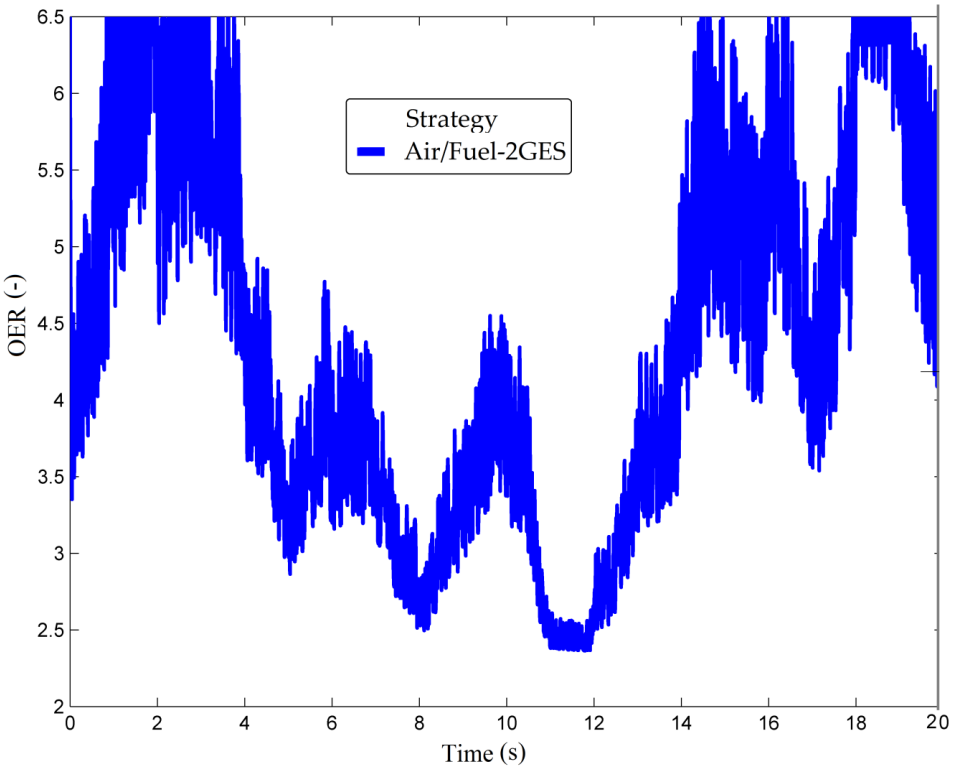

Figure 19. Oxygen excess ratio for FC RES HPS with k_{RES} = 1 and Air/Fuel-2GES strategy.

3.5. FC Net Power Requested from FC RES HPS with k_{RES} = 0 and k_{RES} = 1

FC net power requested to sustain the DC power flow balance of FC RES HPS with k_{RES} = 0 and k_{RES} = 1 are presented in Figures 20 and 21 for all strategies analyzed in this study.

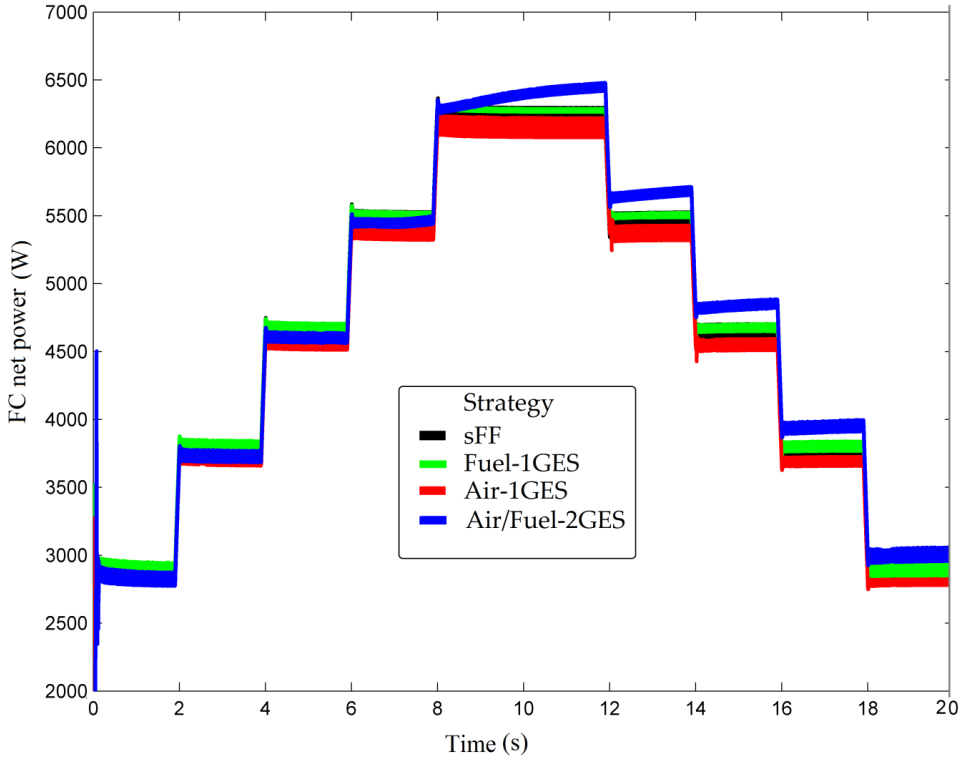

Figure 20. FC net power requested from FC RES HPS with $k_{RES} = 0$.

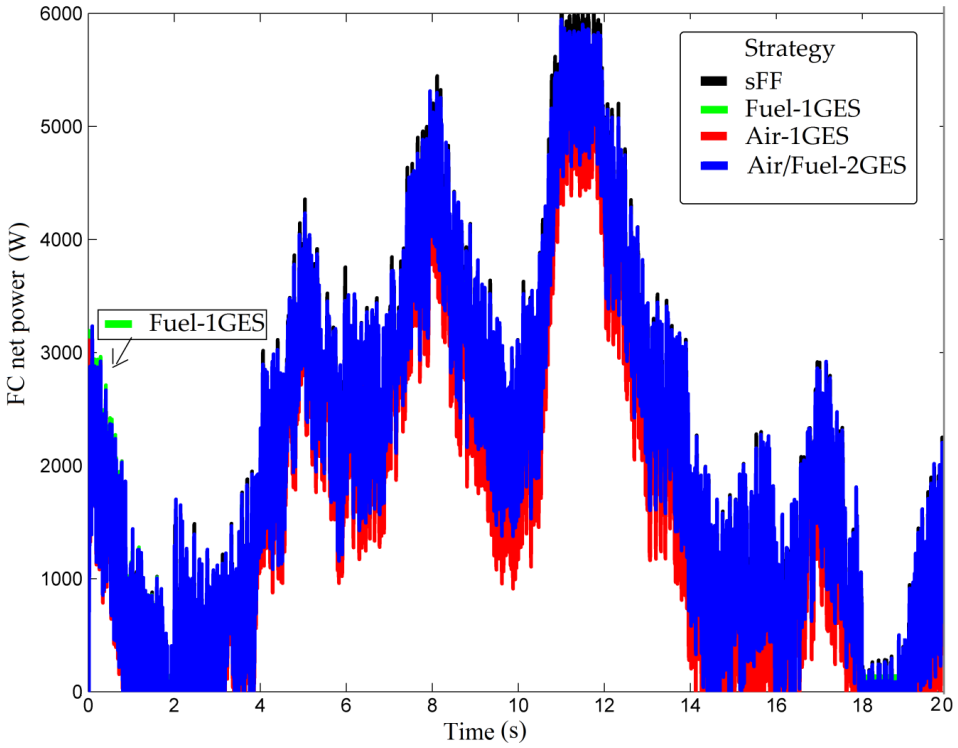

Figure 21. FC net power requested from FC RES HPS with $k_{RES} = 1$.

One issue that may be of interest in using these strategies, which are part of the class of strategies that use the same setting, is whether it can be identified based on the measurements made.

In addition to other discussions of the results obtained, the next section will show how to identify whether the strategy uses one or two GES controllers by simply processing the fuel consumption measurements for HPS with $k_{RES} = 0$ and $k_{RES} = 1$.

4. Discussion

The results obtained for HPS with $k_{RES} = 0$ and $k_{RES} = 1$ in Sections 3.1 and 3.2 are summarized in Tables 4 and 5, where other indicators have been calculated and discussed below.

Table 4. Fuel consumption for FC RES HPS with $k_{RES} = 0$ and $k_{RES} = 1$.

Parameter (Unit) \ Strategy	sFF	Fuel-1GES	Air-1GES	Air/Fuel-2GES SW	Air/Fuel-2GES
$Fuel_{T(strategy)}$ (liters)	286.5	278.4	279.4	275.2	274
$Fuel^{RES}_{T(strategy)}$ (liters)	123.6	113.9	114.1	107.6	108.2
$Fuel_{T(strategy)} - Fuel^{RES}_{T(strategy)}$ (liters)	162.9	164.5	165.3	167.6	165.8
$\frac{Fuel^{RES}_{T(strategy)}}{Fuel_{T(strategy)}}$ (%)	43.14	40.91	40.84	39.10	39.49

Table 5. Fuel economy for FC RES HPS with $k_{RES} = 0$ and $k_{RES} = 1$.

Parameter (Unit) \ Strategy	Fuel-1GES	Air-1GES	Air/Fuel-2GES SW	Air/Fuel-2GES
$\%Fuel_{T(strategy)}$ (%)	2.83	2.48	3.94	4.36
$\%Fuel^{RES}_{T(strategy)}$ (%)	7.85	7.69	12.94	12.46
$\%Fuel^{RES}_{T(strategy)} - \%Fuel_{T(strategy)}$ (%)	5.02	5.21	9.00	8.10
$\frac{\%Fuel^{RES}_{T(strategy)}}{\%Fuel_{T(strategy)}}$ (-)	2.78	3.10	3.28	2.86

Ratio $\frac{Fuel^{RES}_{T(strategy)}}{Fuel_{T(strategy)}}$ was in range of 39.1 to 40.91 for the strategies analyzed in this study (Fuel-1GES, Air-1GES, Air/Fuel-2GES SW and Air/Fuel-2GES), highlighting the contribution of RESs to DC power flow balance compared to load demand (measured by the ratio between the average values of these powers).

If the dependency relationship is chosen linearly, then $\frac{Fuel^{RES}_{T(strategy)}}{Fuel_{T(strategy)}} \cong 1.2 \cdot \frac{P_{load(AV)} - P_{RES1(AV)}}{P_{load(AV)}} - 0.2$. This is verified in two points, as follows:

$$P_{load(AV)} = 5\ kW, P_{RES1(AV)} = 0 \Rightarrow 1 = \frac{Fuel^{RES}_{T(strategy)}}{Fuel_{T(strategy)}} \cong 1.2 \cdot \frac{P_{load(AV)} - P_{RES1(AV)}}{P_{load(AV)}} - 0.2 = 1.2 \cdot \frac{5}{5} - 0.2 = 1 \quad (21)$$

$$P_{load(AV)} = 5\ kW, P_{RES1(AV)} = 2.5\ kW \Rightarrow 0.4 \cong \frac{Fuel^{RES}_{T(strategy)}}{Fuel_{T(strategy)}} \cong 1.2 \cdot \frac{P_{load(AV)} - P_{RES1(AV)}}{P_{load(AV)}} - 0.2 = 1.2 \cdot \frac{5-2.5}{5} - 0.2 = 0.4 \quad (22)$$

Minor differences between the ratio's values obtained with each strategy do not help to define some subclasses. However, the values obtained (close to 40), which was much higher than the value of 43.14 obtained in the case of sFF strategy, shows that all strategies use a similar technique to reduce fuel consumption.

Fuel economy for FC RES HPS with $k_{RES} = 0$ and $k_{RES} = 1$ is computed in Table 5 as percent from fuel consumption using sFF strategy.

Ratio $\frac{\%Fuel^{RES}_{T(strategy)}}{\%Fuel_{T(strategy)}}$ was in range of 2.78 to 3.28 for strategies analyzed in this study, highlighting the same thing as the $\frac{Fuel^{RES}_{T(strategy)}}{Fuel_{T(strategy)}}$ ratio (the contribution of RESs to DC power

flow balance compared to load demand). In this case, the linear dependence is given by $\frac{\%Fuel^{RES}_{T(strategy)}}{\%Fuel_{T(strategy)}} \cong 2.2 \cdot \frac{P_{load(Max)}-\left(P_{load(AV)}-P_{RES1(AV)}\right)}{P_{load(Max)}-P_{load(AV)}} - 1.2$.

Considering $P_{load(Max)} = \eta_{boost} \cdot P_{FCnet(Max)} \cong 7.6\ kW$, this relation is verified in two points, as follows:

$$P_{load(AV)} = 5\ kW, P_{RES1(AV)} = 0 \Rightarrow 1 = \frac{\%Fuel^{RES}_{T(strategy)}}{\%Fuel_{T(strategy)}} \cong 2.2 \cdot \frac{P_{load(Max)}-\left(P_{load(AV)}-P_{RES1(AV)}\right)}{P_{load(Max)}-P_{load(AV)}} - 1.2 = 2.2 \cdot 1 - 1.2 = 1 \quad (23)$$

$$\begin{aligned} &P_{load(AV)} = 5\ kW, P_{RES1(AV)} = 2.5\ kW \Rightarrow \\ &\Rightarrow 3 \cong \frac{\%Fuel^{RES}_{T(strategy)}}{\%Fuel_{T(strategy)}} \cong 2.2 \cdot \frac{P_{load(Max)}-\left(P_{load(AV)}-P_{RES1(AV)}\right)}{P_{load(Max)}-P_{load(AV)}} - 1.2 = 2.2 \cdot \frac{7.6-(5-2.5)}{7.6-5} - 1.2 \cong 3.115 \end{aligned} \quad (24)$$

However, the difference $\%Fuel^{RES}_{T(stategy)} - \%Fuel_{T(stategy)}$ clearly shows that two subclasses can be defined: (1) the class of the strategies Fuel-1GES, Air-1GES (which use one GES controller) and (2) the class of the strategies Air/Fuel-2GES SW and Air/Fuel-2GES (which use two GES controllers). It is worth mentioning that the fuel economy was biggest when using Air/Fuel-2GES SW or Air/Fuel-2GES strategies because these use two GES controllers instead of one. This means a search with two variables in a larger search space.

Other findings of the study performed for HPS with $k_{RES} = 0$ and $k_{RES} = 1$ in Sections 3.1 and 3.2 were the following:

- If the power to be generated by the FC system is small (mainly between 0 and P_{ref}) and a single GES controller strategy is used, then the Air-1GES strategy is recommended. Otherwise, Fuel-1GES strategy is recommended;
- If the power to be generated by the FC system is higher (mainly between P_{ref} and $P_{FC(max)}$) and two GES controllers are used, then the Air/Fuel-2GES strategy is recommended. Otherwise, Air/Fuel-2GES SW strategy is recommended;
- The battery pack operates in charge-sustaining mode if PTC is used for a strategy applied to HPS under dynamic load cycle, without or without RES power; and
- Even if the differences in fuel economy are not major, the definition of specific indicators mentioned above can classify strategies into subclasses or estimate fuel consumption.

The main findings of the study performed for HPS with $k_{RES} = 0$ and $k_{RES} = 1$ in Sections 3.3 and 3.4 were the following:

- The safe operation of HPS is ensured by each analyzed strategy, even in conditions of high load dynamic and large variations of renewable energy power;
- FC net power requested to sustain the DC power flow balance of FC RES HPS under dynamic load cycle and variation of RES power is almost the same due to the optimal value found by each strategy in the search region, which is limited around the current value of the current FC; so these optimal values are close to each other.

This problem of recognizing subclasses of performance from the same class of optimization strategies can also arise for FC HPS (i.e., FC vehicles) by considering two different load cycles and evaluating the performance indicator $\%Fuel^{load1}_{T(stategy)} - \%Fuel^{load2}_{T(stategy)}$.

Furthermore, taking into account different load cycles, the validity of linear relationships such as those introduced below will be verified for other strategies proposed in the literature:

$$\frac{Fuel^{load1}_{T(strategy)}}{Fuel^{load2}_{T(strategy)}} \cong a_1 \cdot \frac{P_{load1(AV)}}{P_{load2(AV)}} - a_2 \quad (25)$$

$$\frac{\%Fuel^{load1}_{T(strategy)}}{\%Fuel^{load2}_{T(strategy)}} \cong a_3 \cdot \frac{P_{load(Max)} - P_{load1(AV)}}{P_{load(Max)} - P_{load2(AV)}} - a_4 \quad (26)$$

where $Fuel^{load}_{T(strategy)}$ is the fuel consumed during the load cycle, $\%Fuel^{load}_{T(strategy)} = 100 \cdot \left(\frac{Fuel^{load}_{T(reference)} - Fuel^{load}_{T(strategy)}}{Fuel^{load}_{T(reference)}}\right)$ is computed using a reference strategy, and parameters a_i, i = 1–4, are specifically determined for each strategy.

Evaluating these ratios would allow a rough estimate of fuel consumption over a predicted load cycle up to the first refueling station based on the fuel consumption on a standard load cycle or during the previous load cycle. Thus, the warning system would signal when it is necessary to refuel from nearby stations.

5. Conclusions

In this study, four fuel economy strategies that use fuel cell optimization through the control of the fueling regulators in the conditions and one reference strategy were analyzed in the conditions in which all strategies used power tracking control of the fuel cell boost converter.

The performance of a strategy (measured for example by the fuel consumption of the FC system) depended on the level of power required from the FC system during a load cycle. Thus, the energy management unit must have a subsystem for selecting the best strategy based on the current value of the load demand and RES power.

If the optimization strategy uses two GES controllers (extending the search for the optimal in two coordinates), then it is recommended to use the Air/Fuel-2GES SW strategy for $0 < P_{FC} < P_{ref}$, and the Air/Fuel-2GES strategy for $P_{ref} < P_{FC} < P_{FC(max)}$. The percentages of fuel economy for strategies Air/Fuel-2GES SW and Air/Fuel-2GES compared to the reference strategy were of 3.94% and 4.36%, and of 12.94% and 12.46%, in the case of a dynamic load cycle with an average of 5 kW and 2.5 kW.

The next research work will focus on testing if the identified indicator ($\%Fuel^{RES}_{T(stategy)} - \%Fuel_{T(stategy)}$) can recognize subclasses of performance from the same class of optimization strategies. For this, experimental validation to evaluate model accuracy will be performed using the general indicator ($\%Fuel^{load1}_{T(stategy)} - \%Fuel^{load2}_{T(stategy)}$). The results presented in this paper highlight the fact that this approach has great chances of being confirmed.

The use of only ultracapacitors stacks instead of hybrid battery/ultracapacitors ESS will also be analyzed in terms of compensation and size performance for use in FC vehicles.

Author Contributions: Conceptualization, methodology, writing—original draft preparation: N.B.; investigation, writing—reviewing and editing: P.T. and D.G. All authors have read and agreed to the published version of the manuscript.

Funding: This work was partially supported by the International Research Partnerships: Electrical Engineering Thai-French Research Center (EE-TFRC) between King Mongkut's University of Technology North Bangkok and Université de Lorraine under Grant KMUTNB-BasicR-64-17.

Conflicts of Interest: The authors declare no conflict of interest.

References

1. Mirsaeidi, S.; Dong, X.; Said, D.M. Towards hybrid AC/DC microgrids: Critical analysis and classification of protection strategies. *Renew. Sustain. Energy Rev.* **2018**, *90*, 97–103. [CrossRef]
2. Burmester, D.; Rayudu, R.; Seah, W.; Akinyele, D. A review of nanogrid topologies and technologies. *Renew. Sustain. Energy Rev.* **2017**, *67*, 760–775. [CrossRef]
3. International Renewable Energy Agency (IRENA). *Off-Grid Renewable Energy Systems: Status and Methodological Issues*; IRENA: Abu Dhabi, UAE, 2015; Available online: https://www.irena.org/-/media/Files/IRENA/Agency/Publication/2015/IRENA_Off-grid_Renewable_Systems_WP_2015.pdf (accessed on 29 June 2020).
4. Kumar, S.; Krishnasamy, V.; Neeli, S.; Kaur, R. Artificial intelligence power controller of fuel cell based DC nanogrid. *Renew. Energy Focus* **2020**, *34*, 1–9. [CrossRef]
5. Global Energy Review 2020—Analysis-IEA. Available online: https://www.iea.org/reports/global-energy-review-2020 (accessed on 29 October 2020).

6. Anastasiadis, A.G.; Konstantinopoulos, S.A.; Kondylis, G.P.; Vokas, G.A.; Papageorgas, P. Effect of fuel cell units in economic and environmental dispatch of a Microgrid with penetration of photovoltaic and micro turbine units. *Int. J. Hydrogen Energy* **2017**, *42*, 3479–3486. [CrossRef]
7. Pashaei-Didani, H.; Nojavan, S.; Nourollahi, R.; Zare, K. Optimal economic-emission performance of fuel cell/CHP/storage based microgrid. *Int. J. Hydrogen Energy* **2019**, *44*, 6896–6908. [CrossRef]
8. Ullah, S.; Haidar, A.M.A.; Hoole, P.; Zen, H.; Ahfock, T. The Current State of Distributed Renewable Generation, Challenges of Interconnection and Opportunities for Energy Conversion based DC Microgrids. *J. Clean. Prod.* **2020**, *12*, 122777. [CrossRef]
9. Pourbehzadi, M.; Niknam, T.; Aghaei, J.; Mokryani, G.; Shafie-khah, M.; Catalão, J.P.S. Optimal operation of hybrid AC/DC microgrids under uncertainty of renewable energy resources: A comprehensive review. *Int. J. Electr. Power Energy Syst.* **2019**, *109*, 139–159. [CrossRef]
10. Yamashita, D.Y.; Vechiu, I.; Gaubert, J.-P. A review of hierarchical control for building microgrids. *Renew. Sustain. Energy Rev.* **2020**, *118*, 109523–109540. [CrossRef]
11. Bai, W.; Abedi, M.R.; Lee, K.Y. Distributed generation system control strategies with PV and fuel cell in microgrid operation. *Control. Eng. Pract.* **2016**, *53*, 184–193. [CrossRef]
12. Brunaccini, G.; Sergi, F.; Aloisio, D.; Randazzo, N.; Ferraro, M.; Antonucci, V. Fuel cells hybrid systems for resilient microgrids. *Int. J. Hydrog. Energy* **2019**, *44*, 21162–21173. [CrossRef]
13. San Martín, J.I.; Zamora, Z.; San Martín, J.J.; Aperribay, V.; Eguia, P. Hybrid fuel cells technologies for electrical microgrids. *Electr. Power Syst. Res.* **2010**, *80*, 993–1005. [CrossRef]
14. Md Hossain, A.; Roy Pota, H.; Md Hossain, J.; Blaabjerg, F. Evolution of microgrids with converter-interfaced generations: Challenges and opportunities. *Int. J. Electr. Power Energy Syst.* **2019**, *109*, 160–186. [CrossRef]
15. Han, Y.; Chen, W.; Li, Q.; Yang, H.; Zare, F.; Zheng, Y. Two-level energy management strategy for PV-Fuel cell-battery-based DC microgrid. *Int. J. Hydrog. Energy* **2019**, *44*, 19395–19404. [CrossRef]
16. Yu, D.; Zhu, H.; Han, W.; Holburn, D. Dynamic multi agent-based management and load frequency control of PV/Fuel cell/ wind turbine/ CHP in autonomous microgrid system. *Energy* **2019**, *173*, 554–568. [CrossRef]
17. San, G.; Zhang, W.; Guo, X.; Hua, C.; Xin, H.; Blaabjerg, F. Large-disturbance stability for power-converter-dominated microgrid: A review. *Renew. Sustain. Energy Rev.* **2020**, *127*, 109859–109870. [CrossRef]
18. Fahad Zia, M.F.; Elbouchikhi, E.; Benbouzid, M. Microgrids energy management systems: A critical review on methods, solutions, and prospects. *Appl. Energy* **2018**, *222*, 1033–1055.
19. Zhang, Y.; Wei, W. Model construction and energy management system of lithium battery, PV generator, hydrogen production unit and fuel cell in islanded AC microgrid. *Int. J. Hydrogen Energy* **2020**, *45*, 16381–16397. [CrossRef]
20. Bizon, N. Load-following Mode Control of a Standalone Renewable/Fuel Cell Hybrid Power Source. *Energy Convers. Manag.* **2014**, *77*, 763–772. [CrossRef]
21. Bizon, N.; Lopez-Guede, J.M.; Kurt, E.; Thounthong, P.; Mazare, A.G.; Ionescu, L.M.; Iana, G. Hydrogen Economy of the Fuel Cell Hybrid Power System optimized by air flow control to mitigate the effect of the uncertainty about available renewable power and load dynamics. *Energy Convers. Manag.* **2019**, *179*, 152–165. [CrossRef]
22. Zhang, Y.; Wei, W. Decentralized coordination control of PV generators, storage battery, hydrogen production unit and fuel cell in islanded DC microgrid. *Int. J. Hydrog. Energy* **2020**, *45*, 8243–8256. [CrossRef]
23. Bizon, N. Real-time optimization strategy for fuel cell hybrid power sources with load-following control of the fuel or air flow. *Energy Convers. Manag.* **2018**, *157*, 13–27. [CrossRef]
24. SimPowerSystems TM Reference. *Hydro-Québec and the MathWorks*; MathWorks Inc.: Natick, MA, USA, 2010.
25. Bizon, N.; Mazare, A.G.; Ionescu, L.M.; Enescu, F.M. Optimization of the Proton Exchange Membrane Fuel Cell Hybrid Power System for Residential Buildings. *Energy Convers. Manag.* **2018**, *163*, 22–37. [CrossRef]
26. Pukrushpan, J.T.; Stefanopoulou, A.G.; Peng, H. *Control of Fuel Cell Power Systems*; Springer: New York, NY, USA, 2004.
27. Bizon, N.; Kurt, E. Performance Analysis of Tracking of the Global Extreme on Multimodal Patterns using the Asymptotic Perturbed Extremum Seeking Control Scheme. *Int. J. Hydrog. Energy* **2017**, *42*, 17645–17654. [CrossRef]

28. Etouke, P.O.; Nneme, L.N.; Mbihi, J. An Optimal Control Scheme for a Class of Duty-Cycle Modulation Buck Choppers: Analog Design and Virtual Simulation. *J. Electr. Eng. Electron. Control Comput. Sci. JEEECCS* **2020**, *6*, 13–20. Available online: https://jeeeccs.net/index.php/journal/article/view/142 (accessed on 29 June 2020).
29. Nneme, L.N.; Lonla, B.M.; Sonfack, G.B.; Mbihi, J. Review of a Multipurpose Duty-Cycle Modulation Technology in Electrical and Electronics Engineering. *J. Electr. Eng. Electron. Control Comput. Sci. JEEECCS* **2018**, *4*, 9–18. Available online: https://jeeeccs.net/index.php/journal/article/view/101 (accessed on 29 June 2020).
30. Bizon, N.; Thounthong, P.; Raducu, M.; Constantinescu, L.M. Designing and Modelling of the Asymptotic Perturbed Extremum Seeking Control Scheme for Tracking the Global Extreme. *Int. J. Hydrog. Energy* **2017**, *42*, 17632–17644. [CrossRef]
31. Bizon, N.; Thounthong, P. Fuel Economy using the Global Optimization of the Fuel Cell Hybrid Power Systems. *Energy Convers. Manag.* **2018**, *173*, 665–678. [CrossRef]
32. Ramos-Paja, C.A.; Spagnuolo, G.; Petrone, G.; Emilio Mamarelis, M. A perturbation strategy for fuel consumption minimization in polymer electrolyte membrane fuel cells: Analysis, Design and FPGA implementation. *Appl. Energy* **2014**, *119*, 21–32. [CrossRef]
33. Restrepo, C.; Ramos-Paja, C.A.; Girala, R.; Calvente, J.; Romero, A. Fuel cell emulator for oxygen excess ratio estimation on power electronics applications. *Comput. Electr. Eng.* **2012**, *38*, 926–937. [CrossRef]
34. Bizon, N. *Optimization of the Fuel Cell Renewable Hybrid Power Systems*; Springer: London, UK, 2020.
35. Mane, S.; Mejari, M.; Kazi, F.; Singh, N. Improving lifetime of fuel cell in hybrid energy management system by Lure-Lyapunov based control formulation. *IEEE Trans. Ind. Electron.* **2017**, *64*, 6671–6679. [CrossRef]